Linear encoding of the spatiotemporal cat map

B Gutkin, L Han, R Jafari, A K Saremi, and P Cvitanović

Center for Nonlinear Cat Science, School of Cat Physics, Georgia Institute of Technology, Atlanta, GA 30332-0430, USA

E-mail: predrag.cvitanovic@physics.gatech.edu

January 3, 2017

Abstract. This XXX describes XXX

PACS numbers: RECHECK! 02.20.-a, 05.45.-a, 05.45.Jn, 47.27.ed

Submitted to: *Nonlinearity*

1. Introduction

While the technical novelty of this paper is in working out details of an elegant, but very special model of many-particle dynamics (or discretization of a classical d-dimensional filed theory), the vision that motivates it is much broader. We address here the long standing problem of how to describe, by means of discrete symbolic dynamics, the spatiotemporal chaos (or turbulence) in spatially extended systems and strongly nonlinear field theories.

Flows described by partial differential equations are in principle infinite dimensional, and, at first glance, turbulent dynamics that they exhibit might appear hopelessly complex. However, what is actually observed in experiments and simulations is that turbulence is dominated by repertoires of identifiable recurrent vortices, rolls, streaks and the like [23]. Dynamics on a low-dimensional chaotic attractor can be visualized as a succession of near visitations to exact unstable periodic solutions of the equations of motion, interspersed by transient interludes [12] . In the same spirit, the long-term turbulent dynamics of spatially extended systems can be thought of as a sequence of visitations of the repertoire of admissible spatiotemporal patterns, each framed and slightly fuzzed out by a finite spatiotemporal "window." The question we address here is: can states of a strongly nonlinear field theory be described by such repertoires of admissible patterns explored by turbulence? And if yes, what is the likelihood to observe any such pattern?

Such questions have been studied extensively for systems of small spatial extension, where the attractor dimension is relatively small [8, 10, 11, 32, 49]. However, going

from spatially small to spatially infinite systems will require completely new tools. For small systems the long time dynamics can be thought of as motion of a point within an inertial manifold of a moderate dimension. A temporally chaotic system is exponentially unstable with time: double the time, and exponentially more periodic orbits are required to cover its strange attractor to the same accuracy. For large spatial extents, the complexity of the spatial shapes also needs to be taken into account; double the spatial extent in a given direction, and exponentially as many distinct spatiotemporal patterns will be required to describe the repertoire of system's shapes to the same accuracy. The systems whose temporal and spatial correlations decay sufficiently fast, and whose "physical" dimension [15, 18] diverges with system size, are said to be "spatiotemporally chaotic." The observation that for spatiotemporally chaotic systems space and time should be considered on the same footing goes back to Politi and collaborators [17, 33, 34, 43] who, in their studies of propagation of spatiotemporal disturbances in extended systems, discovered that the spatial stability analysis can be put on the same footing as the temporal stability analysis.

One way to capture the essential features of turbulent spatiotemporal motions of a physical flow is offered by coupled map lattice models, in which the spacetime is coarsely discretized, with the dynamics of domains that capture important small-scale spatial structures modeled by discrete time maps (Poincaré sections of a single "particle" dynamics) attached to lattice sites, and the coupling to neighboring sites consistent with the translational and reflection symmetries of the problem. Here we shall follow this path by investigating the Gutkin and Osipov [21] "many-particle" coupled cat maps lattice ("spatiotemporal cat map" for short, in what follows), built from the Anosov-Arnol'd-Sinai cat maps (modeling the Hamiltonian dynamics of individual "particles") at sites of a $(d-1)$-dimensional spatial lattice, linearly coupled to their nearest neighbors. The remarkable feature of the "spatiotemporal cat map" model is that its every solution is uniquely encoded by a linear transformation to the corresponding finite alphabet d-dimensional symbol lattice, a spatiotemporal generalization of the linear code for temporal evolution of a single cat map, introduced in the beautiful 1987 Percival and Vivaldi paper [40].

Within this model, a spatial-temporal "window" into system dynamics is provided by a finite block of symbols, and the central question is to understand which symbol blocks are admissible, and what is the likelihood of a given block's occurrence. It was already noted in [21] that two spatiotemporal orbits sharing the same finite block of symbols shadow each other exponentially well within the corresponding spatial-temporal "window". This is the key property of hyperbolic spatiotemporal dynamics that we explore in detail in this paper. The linearity of the spatiotemporal cat map enables us to go far analytically. By using Green's function methods we are able to analytically compute the likelihoods of a large set of spatiotemporally finite blocks, and give an algorithm for exact computation of the rest (so far computationally feasible only for small blocks).

The paper is organized as follows: In section 2 we formulate our central problem

and state the main results of the paper. In section 3 we collect all symbolic dynamics definitions needed forsed throughout the paper. In section 4 we introduce the single cat map, and its linear code formulation (section 4.4). The new results follow from our determination of frequencies of winding numbers generated by the iterations of cat maps, for different integer values of the stretching parameter s. In section 4.5 we investigate frequencies the admissible symbolic sequences, and in section 4.6 we demonstrate the splitting of the alphabet into internal and exterior parts, and show that block frequencies factorize into a "geometric" part, and a constant part which depends only on the length of the block. These frequencies enable us to find the areas of partitions in phase space labelled by the admissible words of cat map symbolic dynamics. We evaluate explicitly the geometrical factor for short blocks of symbols and estimate the single cat map metric entropy.

In sections 1.1 and 5 we extend these results to spatiotemporally 2-dimensional spatiotemporal cat maps, and in section 5.2 show that the linear code offers a natural bridge to spatially and temporally infinite lattices. We then apply these methods to computation of the frequencies of finite spatiotemporal symbol blocks for spatiotemporal cat maps. In section 6 we use these results for construction of families of spatio-temporal periodic solutions shadowing each other at every space-time point. Implementing this program requires new tools, not standard in dynamicists' tool box: new kinds of discrete Green's functions, new kinds of determinants, new relations between propagation of temporal vs. spatial disturbances; some of these are derived in Appendix A. The results are summarized and some open questions discussed in the section 7.

1.1. The model: spatiotemporal cat map

Consider a linear, area preserving map of a 2-torus onto itself

$$\begin{pmatrix} x_{t+1} \\ p_{t+1} \end{pmatrix} = A \begin{pmatrix} x_t \\ p_t \end{pmatrix} \mod 1\,, \qquad A = \begin{pmatrix} s-1 & 1 \\ s-2 & 1 \end{pmatrix}\,, \tag{1}$$

where both x_t and p_t belong to the unit interval. For integer $s = \mathrm{tr}\, A > 2$ the map is referred to as a cat map [3]. It is a fully chaotic Hamiltonian dynamical system, which, rewritten as a 2-step difference equation in (x_t, x_{t-1}) takes a particularly simple form [40]

$$x_{t+1} - s\, x_t + x_{t-1} = -m_t\,, \tag{2}$$

with a unique integer "winding number" m_t at every time step t ensuring that x_t lands in the unit interval. While the force is linear, the nonlinearity comes through the (mod 1) operation, encoded in $m_t \in \mathcal{A}$, where $\mathcal{A}$ is finite alphabet of possible values for m_t.

A generalization to the *spatiotemporal* cat map is now immediate. Consider a 1-dimensional spatial lattice, with field $x_{n,t}$ (the angle of a kicked rotor "particle" at instant t) at site n. If each site couples only to its nearest neighbors $x_{n\pm1,t}$, and if we require (1) invariance under spatial translations, (2) invariance under spatial reflections, and

(3) invariance under the space-time exchange, we arrive at the 2-dimensional Euclidean cat map lattice:

$$x_{n,t+1} + x_{n,t-1} - s\,x_{n,t} + x_{n+1,t} + x_{n-1,t} = -m_{n,t}\,. \tag{3}$$

Note that both equations (2), (3) can be brought into uniform notation and generalized to d dimensions by converting the spatialtemporal differences to discrete derivatives. This yields the Newton (or Lagrange) equation for the d-dimensional *spatiotemporal cat map*

$$(-\Box + s - 2d)x_z = m_z\,, \qquad x_z \in \mathbb{T}^1\,, \quad m_z \in \mathcal{A}\,, \quad z \in \mathbb{Z}^d\,, \tag{4}$$

where $\Box$ is the discrete d-dimensional Euclidean space-time Laplacian, given by $\Box\, x_t \equiv x_{t+1} - 2x_t + x_{t-1}$, $\Box x_{n,t+1} \equiv x_{n,t+1} + x_{n,t-1} - 4\,x_{n,t} + x_{n+1,t} + x_{n-1,t}$ in $d = 1$ and $d = 2$ dimensions, respectively. The key insight (an insight that applies to all coupled-map lattices, and all PDEs modeled by them, not only the system considered here) is that a d-dimensional spatiotemporal pattern $\{x_z\} = \{x_z, z \in \mathbb{Z}^d\}$ requires *d-dimensional* spatiotemporal block $\{m_z\} = \{m_z, z \in \mathbb{Z}^d\}$, rather than a *single* temporal symbol sequence (as one is tempted to do when describing a finite coupled N^{d-1}-"particle" system).

As the relation (4) between the trajectory x_z and its symbolic dynamics encoding m_z is linear, we refer to m_z as the "linear code" [40], both for the cat map (2) in one dimension (temporal dynamics of a single "particle") and for the spatiotemporal cat map (4) in d dimensions (temporal dynamics of a (d-1)-dimensional spatial lattice of N^{d-1} interacting "particles," $N \to \infty$). Linearity of (4) enables us to solve for $\{x_z\}$ given $\{m_z\}$ by lattice Green's function methods. However, dependence on the parameter s introduces an infinite set of grammar rules for admissible itineraries $\{m_z\}$. In this paper we focus on the $d = 1$ case (introduced in [40]), and the $d = 2$ case (introduced in [21]).

2. Overview of the main results

Let $\mathsf{X} = \{x_z \in \mathbb{T}^1\,,\ z \in \mathbb{Z}^2\}$ be a spatiotemporally infinite solution of (4) for $d = 2$, in the fully hyperbolic regime $s > 4$, and let $\mathsf{M} = \{m_z \in \mathcal{A}\,,\ z \in \mathbb{Z}^2\}$ be its symbolic representation. X, being a solution, is by definition an admissible spatiotemporal block. By the linear connection between X and M, the corresponding symbolic dynamics block M is unique and admissible, i.e., M defines the unique spatiotemporal state X and vice-versa. Assume now that only partial information is available, and we know only a local block of symbols $\mathsf{M}_\mathcal{R} \subset \mathsf{M}$ over a finite lattice region $\mathcal{R} \subset \mathbb{Z}^2$. Can we still get information on the local spatiotemporal pattern $x_z, z \in \mathcal{R}$? To be more specific, let $\mathcal{R}$ be a rectangular $[\ell_1 \times \ell_2]$ region (see (13) for details) and let $\mathsf{M}_\mathcal{R}$ be the $[\ell_1 \times \ell_2]$ block of M symbols restricted to $\mathcal{R}$. For the standard symbolic dynamics based on the Markov partition of the cat map phase space, a finite block of symbols defines the corresponding trajectory points up to an error which decreases exponentially with the length of the symbol block [4, 5, 44]. We would like to know whether a similar result holds for 2D

linear symbolic dynamics.

Q1. *To what precision does* $\mathsf{M}_{\mathcal{R}}$ *define the values of* $x_z, z \in \mathcal{R}$*?*

The central question studied in this paper is about the frequency of occurrence of given finite symbols block within the symbolic representations of a generic spatiotemporal pattern. Let $\mathsf{M}_{\mathcal{R}}$ be a fixed $[\ell_1 \times \ell_2]$ block of symbols from the alphabet $\mathcal{A}$.

Q2. *How often does a prescribed finite symbol block* $\mathsf{M}_{\mathcal{R}}$ *occur in the symbolic representation* M *of a generic trajectory* X*?*

Let $\mathcal{N}(\mathsf{M}_{\mathcal{R}}|\mathsf{M}_{[N\times T]})$ be the number of times a given symbol block $\mathsf{M}_{\mathcal{R}}$ appears within a much larger symbol block $\mathsf{M}_{[N\times T]}$ taken from a generic solution M of equation (4). The frequency of the block $\mathsf{M}_{\mathcal{R}}$ is then defined as the limit:

$$\mu(\mathsf{M}_{\mathcal{R}}) := \lim_{N\to\infty, T\to\infty} \mathcal{N}(\mathsf{M}_{\mathcal{R}}|\mathsf{M}_{[N\times T]})/NT\,, \qquad \sum_{\mathsf{M}_{\mathcal{R}}} \mu(\mathsf{M}_{\mathcal{R}}) = 1\,. \tag{5}$$

This definition provides a numerical way to evaluate $\mu(\mathsf{M}_{\mathcal{R}})$ by generating solutions of (4) on finite $[N \times T]$ regions, with random initial conditions, and counting the number of times $\mathsf{M}_{\mathcal{R}}$ occurs within each such solution. On the other hand, if the ergodicity theorem holds, the frequencies $\mu(\mathsf{M}_{\mathcal{R}})$ are the natural measures $\mu(V_{\mathsf{M}_{\mathcal{R}}})$ of the cylinder sets $V_{\mathsf{M}_{\mathcal{R}}}$, defined as sets of phase space points having $\mathsf{M}_{\mathcal{R}}$ symbolic representation over the region $\mathcal{R}$.

In principle, having answers to Q1 and Q2 allows for a calculation of observables by means of symbolic dynamics. Assuming that $\mathsf{M}_{\mathcal{R}}$ defines positions of points in the center z_0 of $\mathcal{R}$ with exponential precision, any local observable A can be seen as essentially a function of $\mathsf{M}_{\mathcal{R}}$. In other words, $A(z_0) \approx A\,(\mathsf{M}_{\mathcal{R}})$, where the quality of the approximation increases exponentially with the size of $\mathcal{R}$. In the limit of large region size $|\mathcal{R}|$ one approximates the sum over states of the lattice with exponentially increasing accuracy, and has for the average of A

$$\langle A\rangle = \lim_{|\mathcal{R}|\to\infty} \sum_{\mathsf{M}_{\mathcal{R}}} \mu(\mathsf{M}_{\mathcal{R}}) A\,(\mathsf{M}_{\mathcal{R}})\ ,$$

where the sum is over all possible combinations of symbols within $\mathcal{R}$. In particular, for $A = -\frac{1}{|\mathcal{R}|}\log\mu(\mathsf{M}_{\mathcal{R}})$ the above expression defines the spatiotemporal entropy of the system.

Main results. The linear code has no simple, finite set of grammar rules. Nevertheless, the spatiotemporal cat map alphabet is finite and we show that can be split into two parts,

$$\mathcal{A} = \mathcal{A}_0 \cup \mathcal{A}_1\,,$$

where the number of symbols in $\mathcal{A}_1$ is finite, and the number of symbols in $\mathcal{A}_0$ grows linearly with s. The significance of this separation stems from the fact that the "inner" part $\mathcal{A}_0$ of the alphabet is a full shift. The following hold for $\mathcal{A}_0$:

- Any block of symbols from $\mathcal{A}_0$ is admissible.
- Frequencies of blocks $\mathsf{M}_\mathcal{R}$ are given by rational numbers and factorize into product of constant and geometrical parts:

  $$\mu(\mathsf{M}_\mathcal{R}) = d_\mathcal{R} F |\mathcal{P}(\mathsf{M}_\mathcal{R})| \,.$$

  The constant $d_\mathcal{R}$ depends only on the shape of $\mathcal{R}$. It is independent of the symbolic content $M_\mathcal{R}$. $|\mathcal{P}(\mathsf{M}_\mathcal{R})|$ can be interpreted as the volume of polytope $\mathcal{P}(\mathsf{M}_\mathcal{R})$ whose dimensions are given by the number of boundary points $|\partial\mathcal{R}|$. For small $\mathcal{R}$, $\mu(\mathsf{M}_\mathcal{R})$ can be evaluated analytically.
- If $\mathsf{M}_\mathcal{R}$ is composed only of symbols from $\mathcal{A}_0$ then $|\mathcal{P}(\mathsf{M}_\mathcal{R})| = 1$ and $\mu(\mathsf{M}_\mathcal{R}) = d_\mathcal{R}$.

In addition, we provide an answer to the question Q1. Namely we show that the block of symbols $\mathsf{M}_\mathcal{R}$ defines the internal points of X up to an error which decreases exponentially with the size of the block $\mathcal{R}$.

- The difference between any solution x_{z_0} of (4) at $z_0 \in \mathcal{R}$ and an "average coordinate" $\bar{x}(\mathsf{M}_\mathcal{R})$ (solely determined by $\mathsf{M}_\mathcal{R}$) is bounded by

  $$|x_{z_0} - \bar{x}(\mathsf{M}_\mathcal{R})| \le C e^{-\nu \ell(z_0, \partial\mathcal{R})} \,, \qquad \nu > 0, \tag{6}$$

  where $\ell(z_0, \partial\mathcal{R})$ is the minimal Euclidean distance between z_0 and the boundary $\partial\mathcal{R}$. An explicit connection between $\bar{x}(\mathsf{M}_\mathcal{R})$ and the block of symbols $\mathsf{M}_\mathcal{R}$ is given in the body of the paper.

Finally, note that all the results above hold for single cat map (i.e., $d = 1$) if $s > 2$. In this case, the region $\mathcal{R}$ is just a string of points with $|\partial\mathcal{R}| = 2$. The resulting regions $\mathcal{P}(\mathsf{M}_\mathcal{R})$ are polygons whose areas can be easily evaluated. It seems to be very plausible that similar results hold for (4) on the lattice of dimension d, provided that the system is in chaotic regime. However, in order to streamline the exposition, we discuss here only the two lowest dimensional cases.

3. Symbolic dynamics: a glossary

Cat maps are but one, very special family of chaotic systems. More generally, analysis of a low-dimensional chaotic dynamical system typically starts [12] with a locally stretching, globally folding flow, such as the Lorentz flow. The flow is then reduced to a discrete time return map by appropriate Poincaré sections. Its state space is partitioned, the partitions labeled by an alphabet, and the qualitatively distinct solutions classified by their temporal symbol sequences. Thus we start our analysis of cat maps by recalling a few standard symbolic dynamics notions, to be used in what follows. The reader can safely skip this section, and return to it later, as needed.

Partitions, alphabets. A division of state space $\mathcal{M}$ into distinct regions $\mathcal{M}_A, \mathcal{M}_B, \ldots, \mathcal{M}_Z$ constitutes a *partition*. Each region is labeled by a symbol m from an N-letter *alphabet* $\mathcal{A} = \{A, B, C, \cdots, Z\}$, where $N = |\mathcal{A}|$ is the number of such regions. Alternatively, one can distinguish different regions by coloring them, with colors serving as the "letters" of the alphabet, as in figure 2. For notational convenience, in alphabets we shall sometimes denote negative m by underlining them, i.e., $\mathcal{A} = \{\underline{2}, \underline{1}, 0, 1\} = \{-2, -1, 0, 1\}$.

Itineraries. For a dynamical system evolving in time, every state space point $x_0 \in \mathcal{M}$ has the *future itinerary*, an infinite sequence of symbols $S^+(x_0) = m_1 m_2 m_3 \cdots$ which indicates the temporal order in which the regions are visited. Given a trajectory $x_1, x_2, x_3, \cdots$ of the initial point x_0 generated by the time-evolution law $x_{n+1} = f(x_n)$, the itinerary is given by the symbol sequence

$$m_n = m \qquad \text{if} \qquad x_n \in \mathcal{M}_m \,. \tag{7}$$

The *past itinerary* $S^-(x_0) = \cdots m_{-2} m_{-1} m_0$ describes the order in which the regions were visited up to arriving to the point x_0. Each point x_0 thus has associated with it the bi-infinite itinerary

$$S(x_0) = S^-.S^+ = \cdots m_{-2} m_{-1} m_0 . m_1 m_2 m_3 \cdots \,, \tag{8}$$

or simply 'itinerary', if we chose not to use the decimal point to indicate the present,

$$\{m_t\} = \cdots m_{-2} m_{-1} m_0 m_1 m_2 m_3 \cdots \tag{9}$$

Shifts. A forward iteration $x \to x' = f(x)$ shifts the entire itinerary to the left through the 'decimal point'. This operation, denoted by the shift operator σ,

$$\sigma(\cdots m_{-2} m_{-1} m_0 . m_1 m_2 m_3 \cdots) = \cdots m_{-2} m_{-1} m_0 m_1 . m_2 m_3 \cdots \,, \tag{10}$$

demotes the current partition label m_1 from the future S^+ to the past S^-. The inverse shift σ^{-1} shifts the entire itinerary one step to the right.

The set of all itineraries that can be formed from the letters of the alphabet $\mathcal{A}$ is called the *full shift*

$$\mathcal{A}^{\mathbb{Z}} = \{(m_k)_{k\in\mathbb{Z}} : m_k \in \mathcal{A} \quad \text{for all} \quad k \in \mathbb{Z}\} \,. \tag{11}$$

The itinerary will be infinite for any trapped (non-escaping) orbit as well as for any non–wandering set orbit (such as an orbit that stays on a chaotic repeller), and infinitely repeating for a periodic trajectory. A map is said to be a 'horseshoe' if its restriction to the non–wandering set is hyperbolic and topologically conjugate to the full $|\mathcal{A}|$-shift.

Lattices. Consider a d-dimensional cubic lattice infinite in extent, with each site labeled by d integers $z \in \mathbb{Z}^d$. Assign to each site z a letter m_z from a finite alphabet $\mathcal{A}$. Any particular fixed choice of letters m_z corresponds to a particular lattice state $\mathsf{M} = \{m_z \in \mathcal{A}\}$, infinite in extent. In other words, a d-dimensional lattice requires a d-dimensional code $\{m_z\} = \{m_{n_1 n_2 \cdots n_d}\}$ for a complete specification of its states.

In the lattice case, the *full shift* is the set of all d-dimensional symbol blocks that can be formed from the letters of the alphabet $\mathcal{A}$

$$\mathcal{A}^{\mathbb{Z}^d} = \{(m_z)_{z\in\mathbb{Z}^d} : m_z \in \mathcal{A} \quad \text{for all} \quad z \in \mathbb{Z}^d\} \,. \tag{12}$$

Multidimensional shifts. By assumption, the evolution law f is of the same form for all times. If the evolution law f is also the same at every lattice site, the group of lattice translations, acting along jth lattice direction by shift σ_j, is a spatial symmetry that commutes with the temporal evolution. A spatiotemporal mapping f that satisfies $f \circ \sigma_j = \sigma_j \circ f$ along the $d-1$ spatial lattice directions is said to be *shift invariant*, with the associate symmetry of dynamics given by the d-dimensional group of discrete spatiotemporal translations.

Blocks. In the case of temporal dynamics, a finite itinerary $\mathsf{M}_{\mathcal{R}} = m_{k+1}m_{k+2}\cdots m_{k+|\mathsf{M}|}$ of symbols from $\mathcal{A}$ is called a *block* of length $|\mathcal{R}|$. More generally, let $\mathcal{R}_z \subset \mathbb{Z}^d$ be a finite $[\ell_1 \times \ell_2 \times \cdots \ell_d]$ "rectangular" lattice region, $\ell_k \geq 1$, whose lower left corner is the $z = (n_1 n_2 \cdots n_d)$ lattice site

$$\mathcal{R} = \mathcal{R}_z^{[\ell_1 \times \ell_2 \times \cdots \ell_d]} = \{(n_1 + j_1, \cdots n_d + j_d) \mid 0 \leq j_k \leq \ell_k - 1\}\,. \tag{13}$$

The associated finite block of symbols $m_z \in \mathcal{A}$ restricted to $\mathcal{R}$, $\mathsf{M}_{\mathcal{R}} = \{m_z | z \in \mathcal{R}\} \subset \mathsf{M}$ is called the block $\mathsf{M}_{\mathcal{R}}$ of volume $|\mathcal{R}| = \ell_1 \ell_2 \cdots \ell_d$.

Periodic orbits, invariant d-tori. A state space point is *periodic* if its orbit returns to it after a finite time T; in shift space the orbit is periodic if its itinerary is an infinitely repeating block p^∞, denoted here by a bar over the finite 'prime' block of symbols.

More generally, a state space point is *spatiotemporally periodic* if it belongs to an invariant d-torus, i.e., a block $\mathsf{M}_{\mathcal{R}}$ that tiles the lattice state M periodically, with period ℓ_j in jth lattice direction.

The set of periodic points $\mathcal{M}_p$ that belong to a given periodic orbit form a *cycle*

$$p = \overline{m_1 m_2 \cdots m_{|p|}} = \{x_{m_1 m_2 \cdots m_{|p|}}, x_{m_2 \cdots m_{|p|} m_1}, \cdots, x_{m_{|p|} m_1 \cdots m_{|p|-1}}\}\,. \tag{14}$$

A *prime* cycle p is a single traversal of the orbit; its label is a block of $|p|$ symbols that cannot be written as a repeat of a shorter block. Each *periodic point* $x_{m_1 m_2 \cdots m_{|p|}}$ is labeled by the starting symbol $m_1 = m_{|p|}$, followed by the next $(|p| - 1)$ steps of its future itinerary.

Generating partitions. A partition is called *generating* if every bi-infinite itinerary corresponds to a distinct point in state space. In practice almost any generating partition of interest is infinite. Even when the dynamics assigns a unique infinite itinerary $\cdots m_{-2}m_{-1}m_0.m_1 m_2 m_3 \cdots$ to each distinct orbit, there generically exist full shift itineraries (11) which are not realized as orbits; such sequences are called *inadmissible*, and we say that the symbolic dynamics is *pruned*.

Subshifts. a dynamical system $(\mathcal{M}, S)$ given by a mapping $f : \mathcal{M} \to \mathcal{M}$ together with a partition $\mathcal{A}$ induces *topological dynamics* (Σ, σ), where the *subshift*

$$\Sigma = \{(m_k)_{k \in \mathbb{Z}}\}\,, \tag{15}$$

is the set of all *admissible* itineraries, and $\sigma : \Sigma \to \Sigma$ is the shift operator (10). The designation 'subshift' comes form the fact that $\Sigma \subset \mathcal{A}^{\mathbb{Z}}$ is the subset of the full shift (11).

Let $\Sigma(\mathsf{M}_{\mathcal{R}})$ be the set of all blocks over $\mathcal{R}$ allowed by the alphabet, and $\Sigma(\mathcal{B})$ is the set of admissible blocks over $\mathcal{R}$.

The principal task in developing the symbolic dynamics of a dynamical system is to determine Σ, the set of all admissible itineraries, i.e., all itineraries that are realized by the given dynamical system.

Pruning, grammars, recoding. If the dynamics is pruned, the alphabet must be supplemented by a *grammar*, a set of pruning rules. Suppose that the grammar can be stated as a finite number of pruning rules, each forbidding a block of finite length,

$$\mathcal{G} = \{b_1, b_2, \cdots b_k\} \ , \tag{16}$$

where a *pruned block* b is a sequence of symbols $b = m_1 m_2 \cdots m_{|b|}$, $m \in \mathcal{A}$, of finite length $|b|$. In this case we can always construct a finite Markov partition by replacing finite length words of the original partition by letters of a new alphabet. In particular, if the longest forbidden block is of length $M+1$, we say that the symbolic dynamics is Markov, a shift of finite type with M-step memory.

Subshifts of finite type. A topological dynamical system (Σ, σ) for which all admissible itineraries are generated by a finite transition matrix

$$\Sigma = \left\{ (m_k)_{k\in\mathbb{Z}} \, : \, T_{s_k s_{k+1}} = 1 \quad \text{for all } k \right\} \tag{17}$$

is called a subshift of *finite type*.

Dynamical partitions. If the symbols outside of given block b remain unspecified,

$$\cdots a_{-2} a_{-1} m_{k+1} m_{k+2} \cdots m_{k+|b|} a_{\ell+1} a_{\ell+2} \cdots \ ,$$

with m_i fixed, and arbitrary $a_i \in \mathcal{A}$, the block labels a contiguous region $\mathcal{M}_b = \mathcal{M}_{m_{k+1} m_{k+2} \cdots m_{k+|b|}}$ in the state space, i.e., the totality of orbits that share common but finite history encoded by the block b. The set of all admissible blocks of length ℓ thus yield a dynamically generated complete partition of the state space, $\mathcal{M} = \cup_b \mathcal{M}_b$.

If a map can be topologically conjugated to a linear map, its symbolic dynamics offers a dramatically simplified description of all admissible solutions of the original flow, with the temporal symbolic dynamics and the state space dynamics related by linear recoding formulas. For example, if a map of an interval, such as a parabola, can be conjugated to a piecewise linear map, the kneading theory [38] classifies *all* of its admissible orbits. Cat maps are linear, but there are several ways of taking advantage of their linearity.

4. A single cat map

Before turning to the many-particle case it is instructive to motivate our spatiotemporal linear code by investigating the single cat map ($N = 1$ particle case; a "spatial lattice" with only one site). As our ultimate goal is semiclassical quantization of a quantum many-particle system (or a quantum field theory), we start by a brief review of the physical origin of cat maps.

Area-preserving maps that describe kicked rotors subject to a discrete time sequence of angle-dependent impulses $F(x_t)$, $t \in \mathbb{Z}$,

$$x_{t+1} = x_t + p_{t+1} \qquad \mod 1, \tag{18}$$

$$p_{t+1} = p_t + F(x_t)\,, \tag{19}$$

play important role in the theory of chaos in Hamiltonian systems, from the Taylor, Chirikov and Greene standard map [7, 35], to the cat maps that we study here. Here $2\pi x$ is the angle of the rotor, p is the momentum conjugate to the configuration coordinate x, $F(x) = F(x+1)$ is periodic with period 1, and the time step has been set to $\Delta t = 1$. Eq. (18) says that in time Δt the configuration trajectory starting at x_t reaches $x_{t+1} = x_t + p_{t+1}\Delta t$, and (19) says that at each kick the angular momentum p_t is accelerated to p_{t+1} by the force pulse $F(x_t)\Delta t$. As the values of x differing by integers are identified, and the momentum p is unbounded, the phase space is a cylinder. However, to analyse the dynamics, one can just as well compactify the state space by folding the momentum dynamics onto a circle (add "mod 1" to (19) as well), and thus reduce the phase space to the 2-torus, and the dynamics to a toral automorphism. The state space is now a $(0,1] \times (0,1]$ square of unit area, with the opposite sides identified.

The simplest example of (18,19) is a rotor subject to a force $F(x) = Kx$ linear in the displacement x. The mod 1 added to (19) makes this a discontinuous "sawtooth," unless K is an integer. In that case the map (18,19) is a Continuous Automorphism of the Torus, or a "cat map" [3], a linear symplectic map on the unit 2-torus state space, $(x \mapsto Ax \,|\, x \in \mathbb{T}^2 = \mathbb{R}^2/\mathbb{Z}^2\,;\; A \in SL(2,\mathbb{Z}))$, with coordinates $x = (x_t, p_t)$ interpreted as the angular position variable and its conjugate momentum at time instant t. Explicitly:

$$\begin{pmatrix} x_{t+1} \\ p_{t+1} \end{pmatrix} = A \begin{pmatrix} x_t \\ p_t \end{pmatrix} \mod 1\,, \qquad A = \begin{pmatrix} a & c \\ d & b \end{pmatrix}\,, \tag{20}$$

where a, b, c, d are integers whose precise values do not matter, as long as $\det A = 1$, so that the map is symplectic (area preserving; the measure $d\mu = dxdp$ is invariant under the cat map action).

A cat map is a fully chaotic Hamiltonian dynamical system if its eigenvalues (stability multipliers) $\Lambda = e^{\lambda}$, $\Lambda^{-1} = e^{-\lambda}$ are real, with the stability exponent $\lambda > 0$. The eigenvalues $\Lambda = (s \pm \sqrt{(s-2)(s+2)})/2$ are functions of a single parameter $s = \mathrm{tr}\, A$, and the map is chaotic if and only if $|s| > 2$. We shall refer here to the least unstable of the cat maps (20), with $s = 3$, as the "Arnol'd," or "Arnol'd-Sinai cat map" [3, 14], and to maps with integer $s > 3$ simply as "cat maps". Cat maps have been extensively analyzed as particularly simple examples of chaotic Hamiltonian dynamics. They exhibit ergodicity, mixing, sensitive dependence on initial conditions (the positivity of the Lyapunov exponent), and local divergence of all trajectories (the positivity of the Kolmogorov-Sinai entropy) [48]. As every Anosov automorphism is topologically conjugate to a linear cat map, detailed understanding of dynamics of cat maps is important also for the much richer world of nonlinear hyperbolic toral automorphisms (for examples, see [9, 16, 47]).

4.1. Adler–Weiss partitions

The above partition strategy works very well for the phase space, symplectic cat maps (20): they admit finite Markov partitions. The standard Adler–Weiss Markov partition for the Arnol'd cat map [1–3] utilizes the stable / unstable directions to define a 3-rectangles generating partition of the torus (see, for example Devaney [9, 14]). It is a subshift of finite type (3 symbols alphabet $\bar{\mathcal{A}}$, with a finite grammar, or a full 5 symbols shift), well suited to the generation and counting of cat map's periodic orbits, with simple rational polynomial formulas for the corresponding topological zeta functions [25]. Rational and irrational initial coordinates generate periodic and ergodic orbits, respectively [29, 41]. Accordingly, points in the phase space can be uniquely labeled by the bi-infinite 1-dimensional itineraries of symbols from $\bar{\mathcal{A}}$, according to their future and past itineraries.

However, for our purposes, Adler–Weiss codes have two shortcomings, and will not be used in this paper: for a single cat map the alphabets have no easy translation to the torus winding numbers, and for N coupled cat maps the size of the alphabet $|\bar{\mathcal{A}}|$ (the number of partitions of the phase space, a $2N$-dimensional unit hypercube) grows exponentially with N. The Percival and Vivaldi [40] *linear code* that we describe next is precisely what will be needed to go from a single cat map to the coupled multi-particle spatial lattice (4).

4.2. Linear code

Eqs. (18,19) are discrete-time Hamilton's equations, which induce temporal evolution on the 2-torus (x_t, p_t) *phase space*. For the problem at hand, it pays to go from the Hamiltonian (x_t, p_t) formulation to the Newtonian (or Lagrangian) (x_t, x_{t+1}) *state space* formulation [40], with p_t replaced by $p_t = (x_t - x_{t-1})/\Delta t$. Eq. (19) then takes the 2-step difference form (the discrete time Laplacian $\Box$ formula for the second order time derivative d^2/dt^2, with the time step set to $\Delta t = 1$),

$$\Box\, x_t \equiv x_{t+1} - 2x_t + x_{t-1} = F(x_t) \qquad \mod 1\,, \tag{21}$$

i.e., Newton's Second Law: "acceleration equals force." For a cat map, with force $F(x)$ linear in the displacement x, the Newton's equation of motion (21) takes form

$$(\Box + 2 - s)x_t = m_t\,, \tag{22}$$

with mod 1 enforced by m_t's, integers from the alphabet $\mathcal{A} = \{\underline{1}, 0, \ldots s-1\}$, necessary to keep x_t for all times t within the unit interval $[0, 1)$.

4.3. Linear code partitions

To interpret m_t's, consider the action of the Newtonian cat map (22) on a 2-dimensional state space point (x_{t-1}, x_t),

$$\begin{pmatrix} x_t \\ x_{t+1} \end{pmatrix} = A' \begin{pmatrix} x_{t-1} \\ x_t \end{pmatrix} - \begin{pmatrix} 0 \\ m_t \end{pmatrix}\,, \qquad A' = \begin{pmatrix} 0 & 1 \\ -1 & s \end{pmatrix}\,. \tag{23}$$

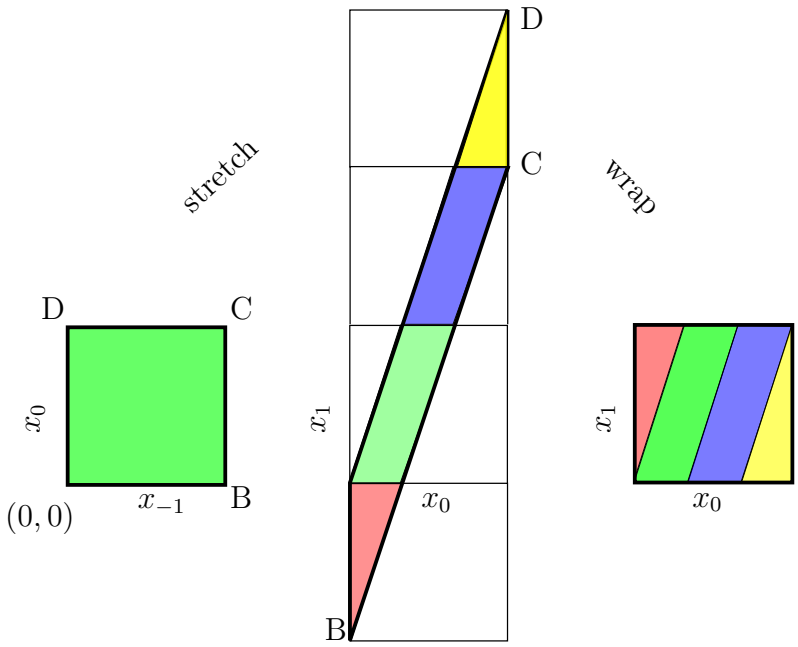

Figure 1. (Color online) The Newtonian $s = 3$ Arnol'd cat map matrix A' (23) keeps the origin $(0, 0)$ fixed, but otherwise stretches the unit square into a parallelepiped. Translations by m_0 from alphabet $\mathcal{A} = \{\underline{1}, 0, 1, 2\}$ = {red, green, blue, yellow} bring stray regions back onto the torus.

As illustrated in figure 1, in one time step the area preserving map A' stretches the unit square into a parallelepiped, and a point (x_0, x_1) within the initial unit square in general lands outside it, in another unit square m_t steps away. As they shepherd such stray points back into the unit torus, the integers m_t can be interpreted as winding numbers [29], or "stabilising impulses" [40]. The m_t translations reshuffle the state space, thus partitioning it into $|\mathcal{A}|$ regions, $\mathcal{M} = \cup\mathcal{M}_m$, $m \in \mathcal{A}$.

Refinements of these partitions work very much like they do for the baker's map and the Smale horseshoe, by peering further into the future and the past, and constructing the intersections of the future and past partitions [12]. The "ℓth level" of partition $\mathcal{M} = \cup\mathcal{M}_b$ is labeled by the set of all admissible blocks b of length ℓ, composed of the past $\ell - t - 1$ steps, and future t steps, with 'decimal point' denoting the present, as in (8),

$$b = m_{t-\ell+1} \cdots m_{-1} m_0 . m_1 m_2 \cdots m_t \, .$$

How the blocks partition the state space is best understood by inspecting figure 2 and figure 3.

4.4. From itineraries to orbits and back

The power of the linear code for a cat map [40] is that one can use integers m_t to encode its state space trajectories. Since the connection (22) between sequences of m_t and x_t is linear, it is straightforward to go back and forth between coordinate and

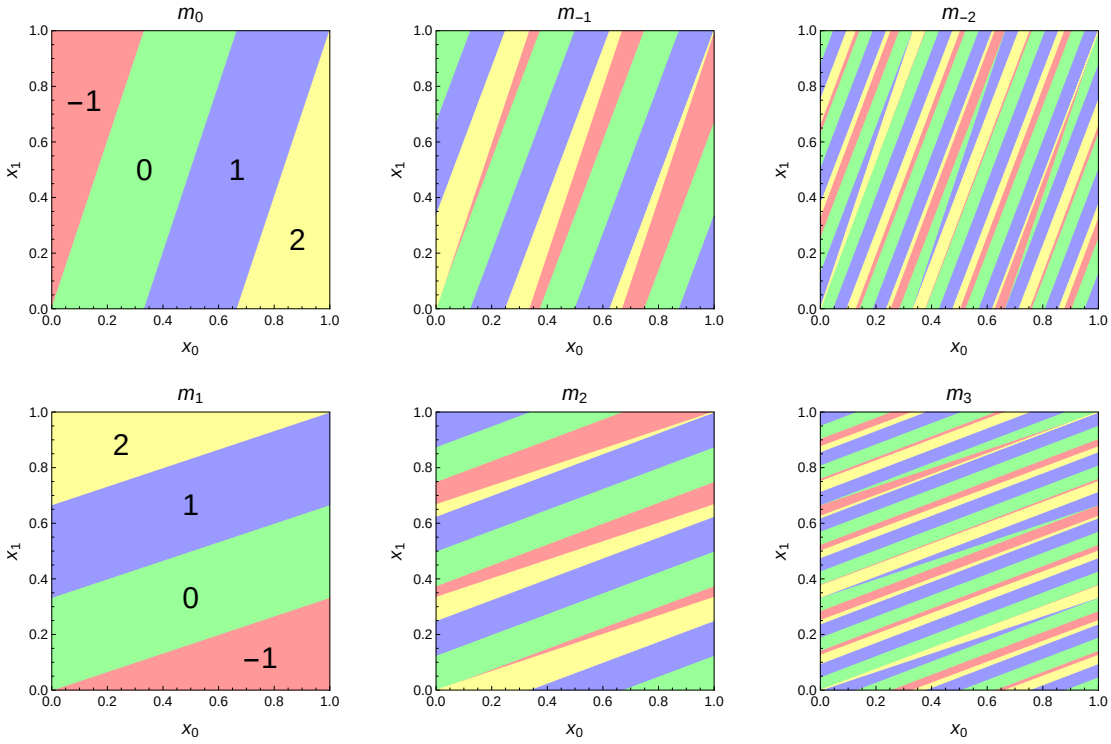

Figure 2. (Color online) Newtonian Arnol'd cat map (x_0, x_1) state space partition into (a) 4 regions labeled by m_0. , obtained from (x_{-1}, x_0) state space by one iteration (the same as figure 1). (b) 14 regions labeled by past block $m_{-1}m_0$. , obtained from (x_{-2}, x_{-1}) state space by two iterations. (c) 44 regions, past block $m_{-2}m_{-1}m_0$. (d) 4 regions labeled by $.m_1$, obtained from (x_2, x_1) state space by one backward iteration. (e) 14 regions labeled by future block $.m_1m_2$, obtained from (x_3, x_2) state space by two backward iterations. (f) 44 regions, future block $m_3m_2m_1$. Each color has the same total area (1/6 for $m_t = \underline{1}, 2$, 1/3 for $m_t = 0, 1$). All boundaries are straight lines with rational slopes.

symbolic representation of trajectories. In particular, if $\{m_t\}$ is an admissible itinerary, the corresponding coordinate at the t time instant is given by the inverse of (22),

$$x_t = \sum_{t'=-\infty}^{\infty} g_{tt'} m_{t'} , \qquad g_{tt'} = \left(\frac{1}{\square + 2 - s} \right)_{tt'} . \tag{24}$$

The matrix $g_{tt'}$ is the Green's function for one-dimensional discretized heat equation [37, 40] whose values are given by $g_{tt'} = \Lambda^{|t-t'|}/(\Lambda - \Lambda^{-1})$, $s = \Lambda + \Lambda^{-1}$ [40], see Appendix A.

In practice one can supply only symbol sequences of finite length, in which case the truncated (24) returns a finite trajectory x_t, with a finite accuracy. However, a periodic orbit p of period n (an n-cycle) is infinite in duration, but specified by a finite admissible block $p = [m_1 m_2 \cdots m_n]$. To generate all admissible n-cycles for a given n, list all prime symbol sequences $[m_1 m_2, \cdots m_n]$, (one string per its n cyclic permutations, not composed from repeats of a shorter cycle), apply (24) with cyclic $[n \times n]$ $g_{tt'}$, and

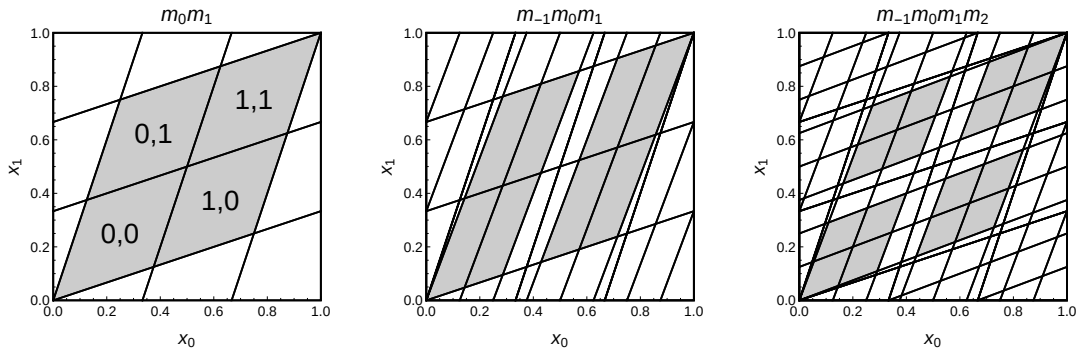

Figure 3. Newtonian Arnol'd cat map (x_0, x_1) state space partition into (a) 14 regions labeled by block $b = m_0.m_1$, the intersection of one past (figure 2 (a)) and one future iteration (figure 2 (d)). (b) block $b = m_{-1}m_0.m_1$, the intersection of two past (figure 2 (b)) and one future iteration (figure 2 (d)). (c) block $b = m_{-1}m_0.m_1m_2$, the intersection of two past (figure 2 (b)) and two future iterations (figure 2 (e)). Note that while some regions involving external alphabet (such as _22_ in (a)) are pruned, the internal alphabet labels a horseshoe, indicated by the shaded regions. Their total area is (a) $4 \times 1/8$, (b) $8 \times 1/21$, and (c) $16 \times 1/55$.

then apply modulus one to all points in the cycle,

$$x_t = \sum_{t'=t}^{n+t-1} g_{tt'} m_{t'} \mod 1 \,. \tag{25}$$

If the cycle is admissible, mod 1 does not affect it. If it is inadmissible, add the string to the list of pruned symbol strings. One can even start with any random sequence $[m_1 m_2 \cdots m_n]$, have mod 1 corral back the stray x_t's into the unit interval, and in this way map any inadmissible symbol sequence into an admissible trajectory of the same duration.

The problem is, as we shall show in section 4.6.4, that for 2-dimensional cat maps the symbolic dynamics is not a subshift of finite type. Thus the linear code cat dynamics is not Markovian, as it grammar consists of an infinity of arbitrarily long pruned (inadmissible) blocks.

Although the recovery of state space periodic orbits from finite symbol string is straightforward for the linear code, it is not easy to describe which symbol sequences are admissible [41]. In contrast to the standard Adler–Weiss Markov partition of the state space cat map, for linear code there is no finite set of short pruned block grammar rules. An itinerary $\ldots m_{-1}m_0m_1 \ldots$ is admissible if and only if each of the corresponding (24) state space orbit points x_t is in the unit interval $[0, 1)$. Therefore, we have an infinite number of conditions to satisfy.

All these conditions are satisfied, however, if the symbols m_t belong to the "inner" alphabet $\mathcal{A}_0 = \{0, \cdots, s-2\}$ which is obtained from $\mathcal{A}$ by the exclusion of two border symbols $\mathcal{A}_1 = \{\underline{1}, s-1\}$. The inner alphabet $\mathcal{A}_0$ is a full shift, meaning that any

sequence of $m_t \in \mathcal{A}_0$ is admissible. Indeed, if $0 \le m_t \le s-2$ for all t, then

$$0 \le \sum_{n=-\infty}^{\infty} \frac{m_n \Lambda^{-|n|}}{\Lambda - \Lambda^{-1}} \le \sum_{n=-\infty}^{\infty} \frac{(\Lambda^{-1} + \Lambda - 2)\Lambda^{-|n|}}{\Lambda - \Lambda^{-1}} = 1\,,$$

and all x_i generated by (24) belong to $[0,1)$. With increasing "stretching" parameter s the number of letters in the inner alphabet $\mathcal{A}_0$ grows as well, while $\mathcal{A}_1$ always contains only two letters. This is consistent with the expectation that in the limit $s \to \infty$ the orbits affected by the outer letters pruning rules can be neglected, and the behavior of the dynamical system should resemble Bernoulli process.

4.5. Frequencies of symbolic sequences

The completeness of linear symbolic code guarantees that an admissible infinite sequence of symbols defines a unique trajectory in the state space. On the other hand, a finite block $b = m_1 m_2 \dots m_\ell$ determines a region $\mathcal{M}_b$ in the state space. More specifically, $\mathcal{M}_b$ is defined as the set of all points having the symbolic representation of the form:

$$\dots a_{-2} a_{-1} m_1 m_2 \dots m_\ell a_{\ell+1} a_{\ell+2} \dots,$$

with m_i's being fixed, while a_i's are arbitrary symbols from $\mathcal{A}$. One is interested in the natural measures $\mu(\mathcal{M}_b)$ of these regions in the state space. By the ergodic theorem the frequency $\mu(b)$ of appearance of block b in a typical trajectory (a.a. with respect to μ) equals to $\mu(\mathcal{M}_b)$. This allows a direct numerical way to evaluate $\mu(\mathcal{M}_b)$ by generating trajectories with random initial conditions.

Let $\{x_i | i \in \mathbb{Z}\}$ be a trajectory generated by the cat map and let $\{m_i | i \in \mathbb{Z}\}$ be its symbolic representation. A coordinate at any moment of time $i \in \{1, \dots \ell\}$ can be expressed through the block $b = m_1 m_2 \dots m_\ell$ at the times $1, \dots \ell$ and the "boundary" coordinates $(x_0, x_{\ell+1})$:

$$x_i = \sum_{j=1}^{\ell} \mathsf{g}_{ij} m_j + \mathsf{g}_{i,1} x_0 + \mathsf{g}_{i,\ell} x_{\ell+1}\,, \qquad i = 1, \dots \ell. \tag{26}$$

Here g is the discrete Green's function with the Dirichlet boundary conditions at $i = 0$ and $i = \ell + 1$. As we show in Appendix A, g_{ij} can be expressed through the Chebyshev polynomials $u_n(s/2) = \sinh(n+1)\lambda / \sinh\lambda$:

$$\mathsf{g}_{ij} = \begin{cases} \frac{u_{i-1}(s/2) u_{\ell-j}(s/2)}{u_\ell(s/2)}, & \text{for } i \le j \\ \frac{u_{j-1}(s/2) u_{\ell-i}(s/2)}{u_\ell(s/2)}, & \text{for } i > j. \end{cases} \tag{27}$$

Note that the first term on the right hand side of (26),

$$\bar{x}_i(b) = \sum_{j=1}^{\ell} \mathsf{g}_{ij} m_j \tag{28}$$

can be thought of as an "approximate" coordinate at time i. Indeed by (26) we have

$$|x_i - \bar{x}_i(b)| = \left| \frac{u_{\ell-i}(s/2)}{u_\ell(s/2)} x_0 + \frac{u_{i-1}(s/2)}{u_\ell(s/2)} x_{\ell+1} \right| \le \frac{\cosh(\frac{1}{2}(\ell+1) - i)\lambda}{\cosh\frac{1}{2}(\ell+1)\lambda}, \tag{29}$$

which implies that the block b determines the coordinate around times $\lfloor \ell/2 \rfloor$ up to an exponentially small error in ℓ. As expected, the minimal error of the order $e^{-\ell\lambda/2}$ occurs at the center of sequence, where $i = (\ell+1)/2$ for odd and $i = (\ell \pm 1 + 1)/2$ for even ℓ, respectively.

As follows from (26), in the coordinate system provided by $(x_0, x_{\ell+1})$ the region $\mathcal{M}_b$ is defined by the following set of inequalities:

$$0 \le \bar{x}_i(b) + \frac{u_{\ell-i}(s/2)}{u_\ell(s/2)} x_0 + \frac{u_{i-1}(s/2)}{u_\ell(s/2)} x_{\ell+1} < 1\,, \qquad i = 1, \dots, \ell, \tag{30}$$

$$0 \le x_0 < 1, \qquad 0 \le x_{\ell+1} < 1\,. \tag{31}$$

In general, this defines a polygon $\mathcal{P}_b$ in the $(x_0, x_{\ell+1})$ plane which is cut out by the straight lines (30) out of the unit square (31). As a result, the measure of the region $\mathcal{M}_b$ and the corresponding frequency of b are given by the product:

$$\mu(b) = \mu(\mathcal{M}_b) = d_\ell |\mathcal{P}_b|, \tag{32}$$

of the Euclidean area $|\mathcal{P}_b|$ of the polygon $\mathcal{P}_b$ and the rescaling factor d_ℓ between the invariant (physical) measure $d\mu = dxdp$ of the state space and the Lebesgue measure $dx_0 dx_{\ell+1}$. In order to find d_ℓ, note that $(x_0, x_{\ell+1})$ are connected with the coordinate and momentum x_k, p_k at a moment of time $k \in (0, \ell+1)$ by:

$$\begin{aligned} x_k &= \bar{x}_k(b) + \frac{u_{\ell-k}(\frac{s}{2})}{u_\ell(\frac{s}{2})} x_0 + \frac{u_{k-1}(\frac{s}{2})}{u_\ell(\frac{s}{2})} x_{\ell+1}, \\ p_k &= \bar{x}_{k+1}(b) - \bar{x}_k(b) + \frac{u_{\ell-k-1}(\frac{s}{2}) - u_{\ell-k}(\frac{s}{2})}{u_\ell(\frac{s}{2})} x_0 + \frac{u_k(\frac{s}{2}) - u_{k-1}(\frac{s}{2})}{u_\ell(\frac{s}{2})} x_{\ell+1}. \end{aligned} \tag{33}$$

Since this is a linear map, d_ℓ is provided by the corresponding Jacobian:

$$d_\ell = \frac{1}{u_\ell^2(\frac{s}{2})} \det \begin{pmatrix} u_{\ell-k-1}(\frac{s}{2}) - u_{\ell-k}(\frac{s}{2}) & u_{\ell-k}(\frac{s}{2}) \\ u_k(\frac{s}{2}) - u_{k-1}(\frac{s}{2}) & u_{k-1}(\frac{s}{2}) \end{pmatrix} = \frac{1}{u_\ell(\frac{s}{2})}. \tag{34}$$

It is important to emphasize that only the geometrical factor $|\mathcal{P}_b|$ in (32) depends on the symbols, while d_ℓ provides normalization independent of b's content.

4.6. Evaluation of frequencies

As the factor d_ℓ is known explicitly the evaluation of $\mu(b)$ hangs on the knowledge of the areas $|\mathcal{P}_b|$. The last one can be easily found analytically in the case of small ℓ. Before looking at specific examples, we list several general properties of $\mu(b)$ which are valid for any ℓ.‡

Symmetries. Symmetries of the cat map induce invariance of f with respect to certain symbol exchanges. For a symbol $m \in \mathcal{A}$ we define its conjugate by $\bar{m} = s - m - 2$. In particular the two exterior symbols from $\mathcal{A}_1$ are conjugate to each other. Let $b = m_1 m_2 \dots m_\ell$ be a sequence of symbols and let $\bar{b} = \bar{m}_1 \bar{m}_2 \dots \bar{m}_\ell$ be its conjugate, then by reflection symmetry of the cat map we have $|\mathcal{P}_b| = |\mathcal{P}_{\bar{b}}|$.

‡ Boris: We should check this section whether it consistent with new convention for symbols

	$\underline{1}$	0	1	2
$\underline{1}$	0	0.0208	0.0625	0.0833
0	0.0209	0.125	0.125	0.0625
1	0.0625	0.125	0.125	0.0209
2	0.0833	0.0625	0.0209	0

$=$

	$\underline{1}$	0	1	2
$\underline{1}$	0	1/48	1/16	1/12
0	1/48	1/8	1/8	1/16
1	1/16	1/8	1/8	1/48
2	1 /12	1/16	1/48	0

Table 1. The frequencies of 2-symbol words $m_i m_{i+1}$ for the Arnol'd cat map $s = 3$, (left) obtained from a long-time numerical simulation; (right) the exact values given by (44), or read off figure 3 (a). Column: m_i. Row: m_{i+1}. Only blocks $\underline{11}$ and 22 are pruned.

Similarly if $m^* = m_l m_{l-1} \dots m_1$, then time reversal invariance implies $|\mathcal{P}_b| = |\mathcal{P}_{b^*}|$. Accordingly, we have

$$\mu(b) = \mu(\bar{b}), \qquad \mu(b) = \mu(b^*). \tag{35}$$

In other words b, b^* and $\bar{b}$ occur with one and the same frequency.

Internal symbols. For sequences which are composed of internal symbols only the inequalities (30) are always satisfied and $\mathcal{P}_b$ are just unit squares with the area 1. The corresponding frequency

$$\mu(b) = \frac{1}{u_{|b|}(\frac{s}{2})}, \qquad m_i \in \mathcal{A}_0, \quad i = 1, \dots |b| \tag{36}$$

depends only on the length of the sequence b.

Rationality. Since all coefficients in (30) are given by rational numbers, the polygon areas $|\mathcal{P}_b|$ are rational too. The same holds for d_ℓ factor. As a result, frequencies $\mu(b)$ are always rational. This allows us to evaluate them exactly, rather than approximately, by integer arithmetic.

Normalization. The sum of all measures $\mu(\mathcal{M}_b)$ for a fixed length $|b|$ should give the total measure of the state space. This implies that for any ℓ:

$$\sum_{|b|=\ell} \mu(b) = 1. \tag{37}$$

4.6.1. Single symbol: $\ell = 1$. For single symbol $m_1 \equiv m$ the set of inequalities (30) reduces to

$$-m \le x_0 + x_2 < s - m. \tag{38}$$

Note that the second constraint is fulfilled automatically for $m \in \mathcal{A}_0$. For $m \in \mathcal{A}_1$, $\mathcal{P}_m$ is the upper and lower triangle, respectively, shown in figure 4 (a). As a result, we have $|\mathcal{P}_m| = 1$ if $m \in \mathcal{A}_0$ and $|\mathcal{P}_m| = 1/2$ if $m \in \mathcal{A}_1$ giving for symbol frequencies:

$$\mu(m) = \begin{cases} 1/s, & \text{for } m \in \mathcal{A}_0 \\ 1/2s, & \text{for } m \in \mathcal{A}_1. \end{cases} \tag{39}$$

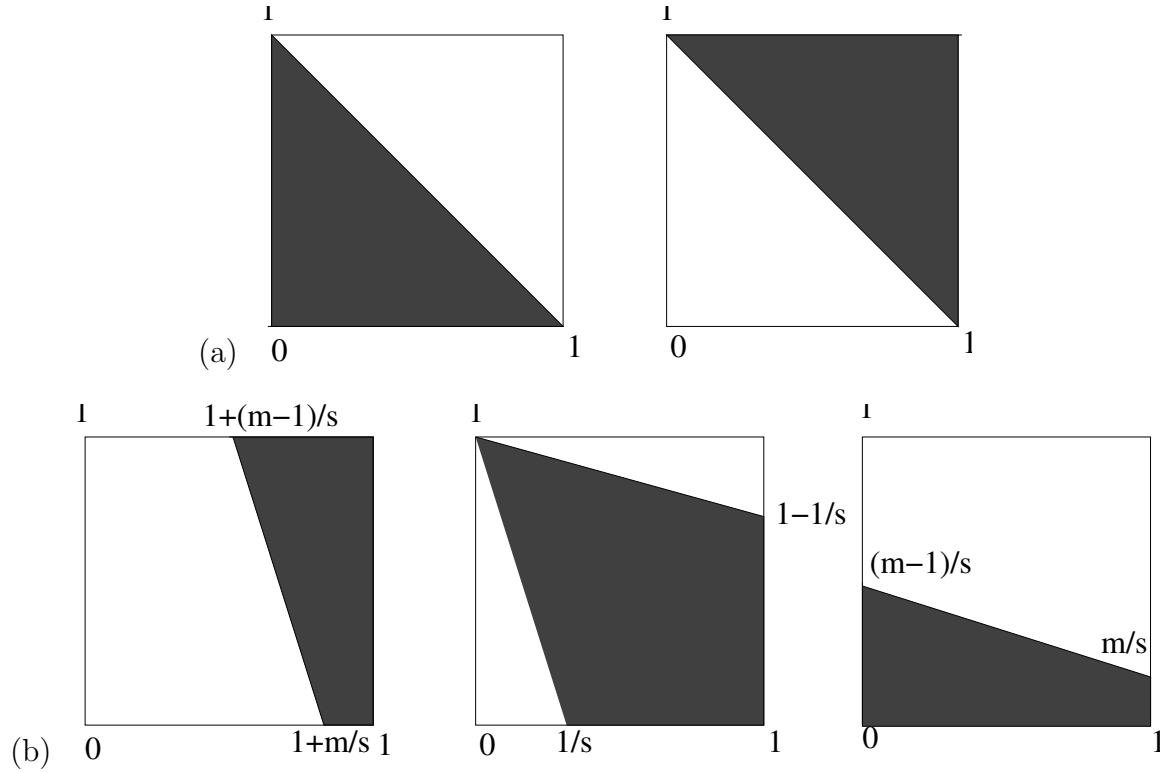

Figure 4. (a) Polygons $\mathcal{P}_m$ (shaded areas) for a single symbol: $m = \underline{1}$ (left), $m = s-1$ (right). (b) Polygons $\mathcal{P}_{m_1 m_2}$ (shaded areas) for blocks of length 2: $m_1 m_2 = \underline{1} m_2,\ m_2 \in \mathcal{A}_0$ (left); $\underline{1} m_2,\ m_2 = s-1$ (middle); $s-1, m_2,\ m_2 \in \mathcal{A}_0$ (right). See also figure 2.

4.6.2. Blocks of length $\ell = 2$: For blocks of length 2, $m_1 m_2$ (30) gives four inequalities

$$-sm_1 - m_2 \le sx_0 + x_3 < s^2 - 1 - sm_1 - m_2 \tag{40}$$

$$-sm_2 - m_1 \le sx_3 + x_0 < s^2 - 1 - sm_2 - m_1. \tag{41}$$

A non-trivial constraint arises when at least one of the symbols belongs to $\mathcal{A}_1$. By the symmetry (35) it is sufficient to analyze the case when $m_1 = \underline{1}$. Assuming that $m_2 \equiv m \in \mathcal{A}_0$ it is easy to see that the region $\mathcal{P}_{-1m}$ is determined by the following conditions, see figure 4 (b):

$$s - m_2 \le sx_0 + x_3, \qquad 0 \le x_0, x_3 < 1. \tag{42}$$

The area of the resulting polygon is equal to $|\mathcal{P}_{\underline{1}m}| = (1+2m)/2s$, where $m \in \mathcal{A}_1$. If both $m_1 \ne m_2$ belong to $\mathcal{A}_1$, i.e., $m_1 = \underline{1}$, $m_2 = s-1$ then the corresponding polygon is determined by the conditions:

$$1 \le sx_0 + x_3, \qquad sx_0 + x_3 \le s, \qquad 0 \le x_0, x_3 < 1. \tag{43}$$

with the corresponding area $|\mathcal{P}_{m_1m_2}| = 1 - 1/s$. Finally, if both m_1, m_2 belong to $\mathcal{A}_1$ and they are equal, then $\mathcal{P}_{m_1m_2} = \emptyset$. As a result we obtain for frequencies:

$$\mu(m_1m_2) = \begin{cases} 1/s^2 - 1 & \text{for } m_1, m_2 \in \mathcal{A}_0 \\ (1+2m_2)/2s(s^2-1) & \text{for } m_1 = \underline{1}, m_2 \in \mathcal{A}_0 \\ 1/s(s+1) & \text{for } m_1 = \underline{1}, m_2 = s-1 \\ 0 & \text{for } m_1 = \underline{1}, m_2 = \underline{1}. \end{cases} \tag{44}$$

The frequencies for the remaining symbol combinations can be obtained by the symmetry (35), see table 1.

4.6.3. Blocks of length ℓ. From (32) the frequency $\mu(b)$ for a block $b = m_1m_2\cdots m_\ell$ is proportional to the area of the polygon defined by inequalities (30). For any cat map with integer $s > 2$, the polygon area $|\mathcal{P}_{m_1m_2\cdots m_\ell}|$ can be evaluated using *Mathematica* geometric computation tools. The full list of frequencies $\mu(m_1m_2\cdots m_\ell)$ has a tensor structure of tensor rank ℓ with each index running over $\mathcal{A}$ and can be interpreted as a joint probability function. Relations that these probabilities must satisfy, such as

$$\sum_{m_1} \mu(m_1m_2\cdots m_\ell) = \mu(m_2\cdots m_\ell), \tag{45}$$

$$\sum_{m_\ell} \mu(m_1m_2\cdots m_\ell) = \mu(m_1\cdots m_{\ell-1}), \tag{46}$$

can be used as consistency checks for the frequency data. In Appendix we list the frequency data for $s = 3$, $\ell = 3$. For $\ell > 3$ such lists of $\mu(m_1m_2\cdots m_\ell)$ get too unwieldy to tabulate here. Instead we look for a visualizations of the frequencies in the (x_0, x_1) plane, by using the dynamical partition of the state space by blocks of length ℓ, as illustrated in figure 2 and figure 3.

Here we emphasize that these partitions are plotted in the (x_0, x_1) state space, in contrast to $(x_0, x_{\ell+1})$ plane of figure 4. As a result, the internal symbol frequencies $\mu(m)$ $(m_i \in \mathcal{A}_0)$ are naturally interpreted as the Jacobian of coordinate transformation from $(x_0, x_{\ell+1})$ to (x_0, x_1):

$$\mu(m) = \frac{1}{u_{|m|}(\frac{s}{2})} = \frac{\partial(x_0, x_1)}{\partial(x_0, x_{\ell+1})}. \tag{47}$$

From the recurrence relation $x_{i+1} = sx_i - x_{i-1} \mod 1$, it is not difficult to establish that $u_{|m|}(\frac{s}{2})$ has the following generating function

$$\sum_{\ell=0} u_{|m|}\left(\frac{s}{2}\right) t^\ell = \frac{1}{1 - st + t^2} \tag{48}$$

$$= 1 + st + (s^2-1)t^2 + (s^3 - 2s)t^3 + \cdots. \tag{49}$$

The number $u_{|m|}(\frac{s}{2})$ is always an integer greater than 1, and the (x_0, x_1) state space is "magnified" and wrapped around the $(x_0, x_{\ell+1})$ phase space $u_{|m|}(\frac{s}{2})$ times through ℓ iterations of the single cat map.

The (x_0, x_1) state space is composed of disjoint unions of regions labelled by all admissible blocks of a fixed length ℓ. As the cat map is invertible, ergodic, and area

Table 2. N_n is the total number of pruned blocks of length $n = |a|$ for the $s = 3$ Arnol'd cat map. $\tilde{N}_n$ is the number of *new* pruned blocks of length $|a|$, with all length $|a|$ blocks that contain shorter pruned blocks already eliminated. Note that (empirically) there is a single new pruning rule for each prime-number period (it is listed as 2 rules, but by the reflection symmetry there is only one).

n	N_n	$\tilde{N}_{n-1}$
2	2	0
3	22	2
4	132	8
5	684	2
6	3164	30
7	13894	2
8	58912	70
9	244678	16
10	1002558	198
11	4073528	2
12	16460290	528
13		2

preserving, it has uniform invariant density $\rho(x_0, x_1) = 1$ and hence the area of each state space region corresponding to a block $b = m_1 m_2 \cdots m_\ell$ equals to its frequency $\mu(b)$. On the other hand, the view from $(x_0, x_{\ell+1})$ phase space has a natural interpretation of area as the relative frequency to sequence of all internal symbols, i.e., the geometrical factor $|\mathcal{P}_m|$. It follows that sequences of internal symbols are maximal possible.

4.6.4. Pruning (**Li - please extend this part**)

As has been previously observed, any sequence of symbols from $\mathcal{A}_0$ is admissible. If, on the other hand, one or more symbols from m belong to $\mathcal{A}_1$ such a sequence might be forbidden i.e., the region $\mathcal{P}_m$ defined by (30,31) is empty and $\mu(m) = 0$. The standard symbolic dynamics for cat maps based on Markov partition has finite grammar rules. These means that pruning rules for symbolic sequences of some finite length define the set of all non-admissible sequences of an arbitrary length. As the results in table 2 show, this is essentially different from the case of linear code. Here the number of new forbidden sequences grows exponentially with ℓ.

4.6.5. Entropy. Given frequencies $\mu(b)$ of blocks b of an arbitrary finite length $|m| = \ell$ one can in principle calculate observables of the dynamical system with an increasing precision as ℓ grows. In the following we apply our central result (32) in order to evaluate metric entropy of the cat map.

The metric entropy of the cat map ϕ with respect to natural measure μ can be represented as the limit

$$h_\mu(\phi) = \lim_{\ell \to \infty} h_\ell, \tag{50}$$

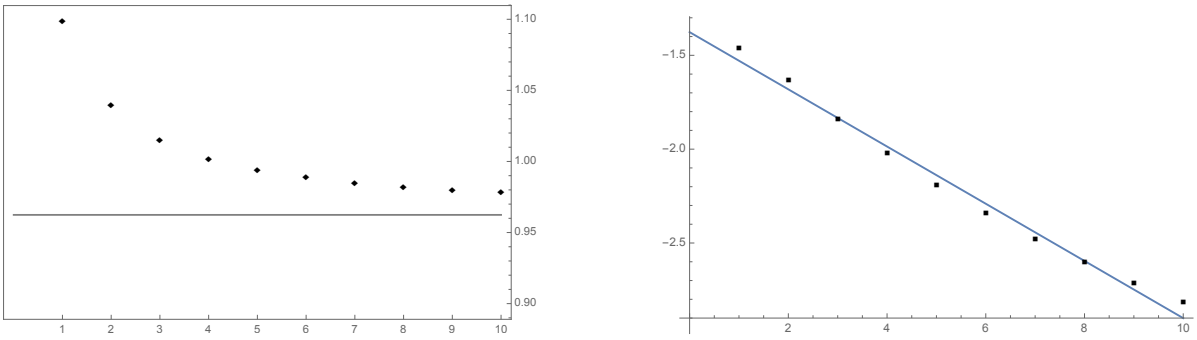

Figure 5. Entropies $\mathcal{S}$ and $\mathcal{S}_{internal}$ vs. the length $|a|$ of periodic orbits used to estimate them. **To Rana: In this figure should be the data for several different s (3 and something) of $\mathcal{S}^1_\ell$**

where

$$h_\ell = -\frac{1}{\ell}\sum_{|b|=\ell} \mu(b)\log\mu(b).$$

By using the decomposition (32) h_ℓ can be split $h_\ell = h^1_\ell + h^0_\ell$ into "geometric" and "internal" parts:

$$h^1_\ell = \frac{\sum_{|b|=\ell} |\mathcal{P}_b| \log |\mathcal{P}_b|}{\ell \sum_{|b|=\ell} |\mathcal{P}_b|}, \qquad h^0_\ell = \frac{1}{\ell}\log u_\ell(s/2).$$

The "inner" part h^0_ℓ converges to $\log\Lambda$ with the rate $O(1/\ell)$. Since $\log\Lambda$ is precisely the value of $h_\mu(\phi)$, the metric entropy [46], it yields for the geometrical part: $\lim_{\ell\to\infty} h^1_\ell = 0$. In figure 5 we verify this directly by numerical calculations for several different s.

5. Spatiotemporal cat map

We now turn to the study of the spatiotemporal cat map (4), with cat maps on sites ("particles") coupled isotropically over a 2-dimensional spatiotemporal $\mathbb{Z}^2$ lattice. In order to motivate this model, we briefly review the early work on coupled map lattices (CMLs), and then describe the new results (the core of this paper) specific to this exceptionally elegant N-"particle" CML.

In order to solve a partial differential equation (PDE) on a computer, one has to represent it by a finite number of computational elements. The simplest discretization of a spacetime field $x(q,\tau)$ is by specifying its values $x_{n,t} = x(q_n,\tau_j)$ on lattice points $(n,t)\in\mathbb{Z}^2$. Once spatial and temporal derivatives are replaced by their discretizations, a PDE has been reduced to a CML, whose conceptual advantage is not only numerical, but also that the technical problems such as existence and uniqueness of PDEs are regularized away, and the essence of spatiotemporal chaos is revealed in a transparent form.

In Euclidean field theory one couples the neighbors harmonically, and thinks of this starting, free field theory formulation as a spring mattress [51] to which then

weakly coupled nonlinear term are added. Similarly, the conventional CML models, mostly motivated by discretizations of dissipative PDEs, start out with chaotic on-site dynamics weakly coupled spatially, with strong space-time asymmetry. An example are diffusive coupled map lattice (CML) models of spatiotemporal dynamics, introduced and simulated numerically by Kaneko [26, 27], with time evolution given by

$$\begin{aligned} x_{n,t+1} &= g(x_{n,t}) + \epsilon\,\frac{1}{2}[g(x_{n-1,t}) - 2g(x_{n,t}) + g(x_{n+1,t})] \\ &= (1 + \epsilon\,\Box)g(x_{n,t})\,, \end{aligned} \tag{51}$$

where the individual spatial site's dynamical system $g(x)$ is a 1D map such as the logistic map, coupled diffusively to its nearest neighbors, and $\Box$ is the spatial version of (21), the Laplacian formula for the discretized second order *spatial* derivative d^2/dx^2, with the lattice spacing constant set equal to unity.

The iteration of a map $g(x_t)$ generates a group of *time translations*. An important class of lattice models consists of those that are also invariant under the group of *space translations* (spatially homogenous). Such models were studied by Bunimovich and Sinai [6] in the case when $g(x_{n,t})$ is a one-dimensional expanding map. For quantum mechanics and statistical mechanics applications, one needs the dynamics to be Hamiltonian, motivating models such as coupled standard map lattice [28] and ϕ^4 lattice [24]. Pesin and Sinai [42] were the first to study a lattice with chains of interacting Anosov maps as a model coupled Hamiltonian maps lattice. In order to established rigorously the desired statistical properties of coupled map lattices, such as the continuity of their SRB measures, they, and all of the subsequent statistical mechanics literature, relied on the structural stability of Anosov automorphisms under small perturbations. For such lattices the neighboring sites have to be coupled sufficiently weakly (small ϵ in (51)) so that the site cat maps could be conjugated to a lattice of uncoupled Anosov automorphisms, with finite Markov partitions, the key ingredient required for the proofs.

By contrast, the spatiotemporal cat map [21] studied here has, in a sense, the temporal and spatial dynamics coupled as strongly as possible. It is model a field theory, where the local degrees of freedom are hyperbolic rather than oscillatory ("inverted pendula"), and as the model is space $\leftrightarrow$ time symmetric, the couplings are the strongest, the most non-perturbative ($\epsilon = 1$ in (51)). And the goals are very different: in this paper we focus on the enumeration of admissible spatiotemporal patterns, and their recurrences (shadowing of large invariant 2-tori by smaller invariant 2-tori).

For a Hamiltonian set of fields we also have $p_{n,j} = p(x_n, t_j)$. In a spatiotemporal cat map, a cat map at each periodic lattice site is coupled diffusively to its nearest neighbors:

$$q_{n,j+1} = p_{n,j} + (s-3)q_{n,j} - (q_{n+1,j} - 2q_{n,j} + q_{n-1,j}) - m^q_{n,j+1}$$

$$p_{n,j+1} = p_{n,j} + (s-4)q_{n,j} - (q_{n+1,j} - 2q_{n,j} + q_{n-1,j}) - m^p_{n,j+1}$$

The spatiotemporal symbols follow from the Newtonian equations in d spatiotemporal

dimensions

$$\begin{aligned} m_{n,j} &= (q_{n,j+1} - 2q_{n,j} + q_{n,j-1}) + (q_{n+1,j} - 2q_{n,j} + q_{n-1,j}) - (s-4)q_{n,j} \\ m &= [\Box + 2(d+1)\mathbf{1} - s\mathbf{1}]\, q\,. \end{aligned} \tag{52}$$

The $[\Box + 2d\,\mathbf{1}]$ is the standard statistical mechanics diffusive inverse propagator that counts paths on a d-dimensional lattice [50], and $-s\mathbf{1}$ is the on-site cat map dynamics.

5.1. Spatiotemporal cat map

The model is defined as a $\mathbb{Z}^1$ chain of linearly coupled cat maps acting on the direct product of the 2-dimensional tori $V = \otimes_n \mathbb{T}^2_n$, $n \in \mathbb{Z}^1$. Each torus $\mathbb{T}^2_n$ is equipped with the phase space coordinate pair $(x_n, p_n) \in (0,1] \times (0,1]$ which determines the position and momentum of the n'th "particle". The spatiotemporal cat map maps $\Phi : V \to V$ generates time evolution of the system in accordance with the rules:

$$\begin{aligned} x_{n,t+1} &= p_{n,t} + a x_{n,t} - x_{n+1,t} - x_{n-1,t} - m^x_{n,t+1} \\ p_{n,t+1} &= b p_{n,t} + (ab-1) x_{n,t} - b\,(x_{n+1,t} + x_{n-1,t}) - m^p_{n,t+1}, \end{aligned} \tag{53}$$

where $x_{n,t}$, $p_{n,t}$ are the coordinate and momentum of the n'th particle at the moment of time t, and $m^x_{n,t}, m^p_{n,t}$ are the corresponding winding numbers necessary to bring $x_{n,t}$, $p_{n,t}$ back to the unit interval. The system is translation invariant under the shift map $\sigma : n \to n+1$ action.

Along with the infinite chain we will consider the finite counterpart of the model, where N cat maps are coupled cyclically. In such a case (53) are subject to the periodic boundary conditions $x_n = x_{n+N}$, $p_n = p_{n+N}$. This defines the map $\Phi_N : V_N \to V_N$ whose action on the $2N$-dimensional phase space $V_N = \otimes_{n=1}^N \mathbb{T}^2_n$ is provided by the linear transformation:

$$Z_{t+1} = \mathcal{B}_N Z_t \bmod 1, \qquad Z_t = (q_{1,t}, p_{1,t}, \ldots q_{N,t}, p_{N,t})^T,$$

with $2N \times 2N$ matrix $\mathcal{B}_N$ given by:

$$\mathcal{B}_N = \begin{pmatrix} A & B & 0 & \ldots & 0 & B \\ B & A & B & \ldots & 0 & 0 \\ 0 & B & A & \ldots & 0 & 0 \\ \vdots & \vdots & \vdots & \ddots & \vdots & \vdots \\ 0 & 0 & 0 & \ldots & A & B \\ B & 0 & 0 & \ldots & B & A \end{pmatrix}, \tag{54}$$

$$A = \begin{pmatrix} a & 1 \\ ab-1 & b \end{pmatrix}, \qquad B = -\begin{pmatrix} 1 & 0 \\ b & 0 \end{pmatrix}.$$

Since the matrix $\mathcal{B}_N$ is symplectic, the map Φ_N preserves the natural measure $d\mu_N = \prod_{i=1}^N dx_i dp_i$ on V_N. In the limit $N \to \infty$, μ_N induces the corresponding measure μ on V which is invariant under both Φ and σ_2.

By the linear structure of Φ_N each invariant 2-torus has one and the same spectrum of the Lyapunov exponents λ_k, $k = 1, \dots 2N$. They are provided by the eigenvalues $\Lambda_k = e^{\lambda_k}$ of the matrix $\mathcal{B}_N$:

$$\Lambda_k + \Lambda_k^{-1} = s - 2\cos(2\pi k/N), \qquad k = 1, \dots N. \tag{55}$$

Accordingly, the map is fully hyperbolic iff $s = a + b > 4$. In this case all solutions of (55) are paired such that $\lambda_k^+ = -\lambda_k^-$ and $\lambda_k^+ > 0$ for all k. The metric entropy of Φ_N for a finite N is given by the sum of all positive exponents:

$$h(\Phi_N) = \sum_{k=1}^{N} \log \lambda_k^+.$$

For the infinite lattice the corresponding spatio-temporal entropy of Φ with respect to μ is given by the limit $h_\mu(\Phi) = \lim_{N\to\infty} \frac{1}{N} h(\Phi_N)$ leading to

$$h_\mu(\Phi) = \frac{1}{\pi^2} \int_0^\pi \int_0^\pi dx\, dy \log(s - 4 + 4\sin^2 x + 4\sin^2 y). \tag{56}$$

5.2. Linear symbolic dynamics

As in the single cat map case, it is instructive to write down equations of motion in the Newtonian form:

$$(\Box + 4 - s)\, x_{n,t} = m_{n,t}, \tag{57}$$

with $\Box$ being the discrete space-time Laplacian on $\mathbb{Z}^2$:

$$\Box\, x_{n,t} := x_{n,t-1} + x_{n,t+1} + x_{n-1,t} + x_{n+1,t} - 4\, x_{n,t}.$$

The symbols $m_{n,t}$'s from the set $\mathcal{A} = \{\underline{3}, \underline{2}, \cdots, s-2, s-1\}$ on the right hand side of (57) are necessary to keep $x_{n,t}$ within the interval $[0, 1)$. As we show below, the block $\{m_{n,t} | (n,t) \in \mathbb{Z}^2\}$ can be used as a 2-D symbolic representation of the system lattice states.

First, we show that any solution of (57) can be uniquely restored from its symbolic representation. By inverting (57) we obtain

$$x_z = \sum_{z' \in \mathbb{Z}^2} g_{zz'} m_{z'}, \qquad g_{zz'} = \left(\frac{1}{\Box + 4 - s} \right)_{zz'}, \tag{58}$$

where $g_{zz'}$ is the Green's function for the 2-dimensional discretized heat equation, see Appendix A. A lattice state $\mathsf{M} = \{m_z | z \in \mathbb{Z}^2\}$ is admissible if and only if all x_z defined by (58) fall into the interval $[0, 1]$.

As for the single cat map, we split the alphabet $\mathcal{A} = \mathcal{A}_0 \cup \mathcal{A}_1$ into the inner $\mathcal{A}_0$ and outer $\mathcal{A}_1$ alphabets

$$\mathcal{A}_0 = \{0, \dots, s-4\}, \quad \mathcal{A}_1 = \{\underline{3}, \underline{2}, \underline{1}\} \cup \{s-3, s-2, s-1\}. \tag{59}$$

If all m_z belong to $\mathcal{A}_0$ then $\mathsf{M} = \{m_z | z \in \mathbb{Z}^2\}$ is a full shift. Indeed, by the positivity of Green's function (see Appendix A) it follows immediately that $0 \le x_z$, while the condition $\sum_{z' \in \mathbb{Z}^2} g_{zz'} = s - 4$ implies that $x_z \le 1$ with the equality reached only if $m_z = s - 4$, for all $z \in \mathbb{Z}^2$.

5.3. Frequencies of symbolic blocks

Let $\mathcal{R} \subset \mathbb{Z}^2$ be a simply connected region on $\mathbb{Z}^2$ with the boundary $\partial\mathcal{R}$ of the length $|\partial\mathcal{R}|$. Take $\mathsf{M}_\mathcal{R} = \{m_z | z \in \mathcal{R}\}$ be a block defined on $\mathcal{R}$. We are going to show now that $\mathsf{M}_\mathcal{R}$ determines approximate positions of the points x_z, $z \in \mathcal{R}$ within the region $\mathcal{R}$. To this end let us consider the equation (57) with the Dirichlet boundary conditions at the boundary $\partial\mathcal{R}$. By Green's theorem (in discretized setting) one gets:

$$x_z = \sum_{z' \in \mathcal{R}} \mathsf{g}_{z,z'} m_{z'} + \sum_{z'' \in \partial\mathcal{R}} \mathsf{g}_{z,z''} x_{z''}, \qquad z \in \mathcal{R}, \tag{60}$$

where $\mathsf{g}_{z,z'}$ is the corresponding Green's function with the Dirichlet boundary conditions, see Appendix A. We define then $\bar{x}_z := \sum_{z' \in \mathcal{R}} \mathsf{g}_{z,z'} m_{z'}$ as an approximate position of x_z. From (60) the difference $|x_z - \bar{x}_z|$ can be bounded by

$$|x_z - \bar{x}_z| = \sum_{z'' \in \partial\mathcal{R}} \mathsf{g}_{z,z'} x_{z''} \leq |\partial\mathcal{R}|\, \mathsf{g}_{\ell_{\min}}, \tag{61}$$

with $\ell_{\min}$ being the minimal distance between $\partial\mathcal{R}$ and z. For a rectangular region of the dimension $\ell_1 \times \ell_2$, and the point z being at the center of $\mathcal{R}$, $\ell_{\min} = \min\{\ell_1/2, \ell_2/2\}$. As for large z the Green's function $\mathsf{g}_{z,z'}$ decays exponentially with $|z - z'|$, the distance $|x_z - \bar{x}_z|$ is of the order $|\partial\mathcal{R}|\, e^{-\lambda\ell_{\min}}$ for a large $\ell_{\min}$.

We are going now to determine frequencies $\mu(\mathsf{M}_\mathcal{R})$ with which $\mathsf{M}_\mathcal{R}$ appears in a.a. (with respect to natural measure) lattice state. To simplify the exposition we assume in what follows that $\mathcal{R}$ is an $\ell_1 \times \ell_2$ rectangular region

$$\mathcal{R} = \{(n_0 + i, t_0 + j) |\, i = 1, \ldots, \ell_1,\ j = 1, \ldots, \ell_2\}\,.$$

In what follows it is convenient to distinguish points in the interior of $\mathcal{R}$ from the points which belong to the boundary $\partial\mathcal{R}$. The later ones will be labeled as z_i, where i runs from 1 to $\mathcal{D} := |\partial\mathcal{R}| = 2(\ell_1 + \ell_2)$ and the corresponding set of the coordinates at the boundary $x_i \equiv x_{z_i}$. Both the boundary coordinates $x_i, i = 1, \ldots \mathcal{D}$ and the internal ones $x_z, z \in \mathcal{R}$ must belong to the unit interval. By (60) this implies:

$$0 \leq x_i < 1, \qquad i = 1, \ldots, \mathcal{D} \tag{62}$$

$$0 \leq \bar{x}_z + \sum_{i=1}^{\mathcal{D}} \mathsf{g}_{z,z_i} x_i < 1, \qquad z \in \mathcal{R}\,. \tag{63}$$

Accordingly, the admissible set of $x_i, i = 1, \ldots \mathcal{D}$ form the region $\mathcal{P}(\mathsf{M}_\mathcal{R})$ in the $\mathcal{D}$-dimensional Euclidean space. Informally speaking, here the second set of inequalities (63) cuts out a polytope out off the $\mathcal{D}$-dimensional unit hypercube defined by (62). As in the case of single cat map, the frequencies $\mu(\mathsf{M}_\mathcal{R})$ can be factorised into product:

$$\mu(\mathsf{M}_\mathcal{R}) = d(\mathcal{R}) |\mathcal{P}(\mathsf{M}_\mathcal{R})|, \tag{64}$$

where $|\mathcal{P}(\mathsf{M}_\mathcal{R})|$ is the volume of the polytope defined by (62) and (63). The first factor $d(\mathcal{R})$ is provided by the Jacobian of the linear connection between boundary coordinates $x_i, i = 1, \ldots \mathcal{D}$ and a subset of the phase space coordinate and momenta on a fixed time line $\{(x_z, p_z), z = (t, n) |\, n = 1, \ldots N\}$.

Since the Jacobian of this transformation is independent of $\mathsf{M}_{\mathcal{R}}$, the factor $d(\mathcal{R})$ is a constant which depends only on the shape of $\mathcal{R}$, but not on its symbolic content.

Remark: Recall that for single cat map the constant $d(\mathcal{R})$ was given explicitly by (34). In the case of spatiotemporal cat map we were unable to extract a similarly simple expression, even in the case of rectangular regions. On the other hand, by the same argument as in the single cat map case, it might be expected that in the limit of large regions $\mathcal{R}$ the asymptotics of $d(\mathcal{R})$ should be determined by the metric entropy. In other words, it might be expected that asymptotically for large regions $\mathcal{R}$:

$$\log d(\mathcal{R}) \sim -|\mathcal{R}|\, h_\mu(\Phi), \qquad \text{as } |\mathcal{R}| \to \infty\,,$$

where $h_\mu(\Phi)$ is the spatiotemporal metric entropy (56) of the spatiotemporal cat map.

5.4. Evaluation of frequencies

We first list the basic properties of the frequencies $\mu(\mathsf{M}_{\mathcal{R}})$ which ar largely mimic their counterparts in the single cat case.

Symmetries. Besides the invariance under shifts in time t and space n directions (57) are invariant invariant under the space and time reflections $n \to -n$, $t \to -t$. In addition, the equation (57) is symmetric under exchange $n \longleftrightarrow t$. This in turn implies that

$$\mu(\mathsf{M}_{\mathcal{R}}) = \mu(g \circ \mathsf{M}_{\mathcal{R}}), \qquad \mu(\mathsf{M}_{\mathcal{R}}) = \mu(\bar{\mathsf{M}}_{\mathcal{R}}), \tag{65}$$

where g is an element of dihedral group D_4 and the bar operation transforms the symbols of M according to the rule $m_{n,t} \to s - m_{n,t} - 4$.

Internal symbols. Note that the set of inequalities (63) is satisfied automatically if all symbols from $\mathsf{M}_{\mathcal{R}}$ belong to $\mathcal{A}_0$. This follows immediately from the positivity of the Green's function $\mathsf{g}_{z,z'}$ and the identity:

$$1 = (s-4)\sum_{z'\in\mathcal{R}} \mathsf{g}_{z,z'} + \sum_{z''\in\partial\mathcal{R}} \mathsf{g}_{z,z''}, \qquad z \in \mathcal{R}. \tag{66}$$

As a result, for any block of internal symbols $|\mathcal{P}(\mathsf{M}_{\mathcal{R}})| = 1$ and the frequency

$$\mu(\mathsf{M}_{\mathcal{R}}) = \frac{1}{d(\mathcal{R})} \tag{67}$$

is independent on the content of $\mathsf{M}_{\mathcal{R}}$.

Rationality. For any $\mathsf{M}_{\mathcal{R}}$, $\mu(\mathsf{M}_{\mathcal{R}})$ is a rational number. This follows from the rationality of each element $\mathsf{g}_{z,z'}$.

Normalization. For a fixed region $\mathcal{R}$:

$$\sum \mu(\mathsf{M}_{\mathcal{R}}) = 1, \tag{68}$$

where the sum is over all possible blocks over the region $\mathcal{R}$.

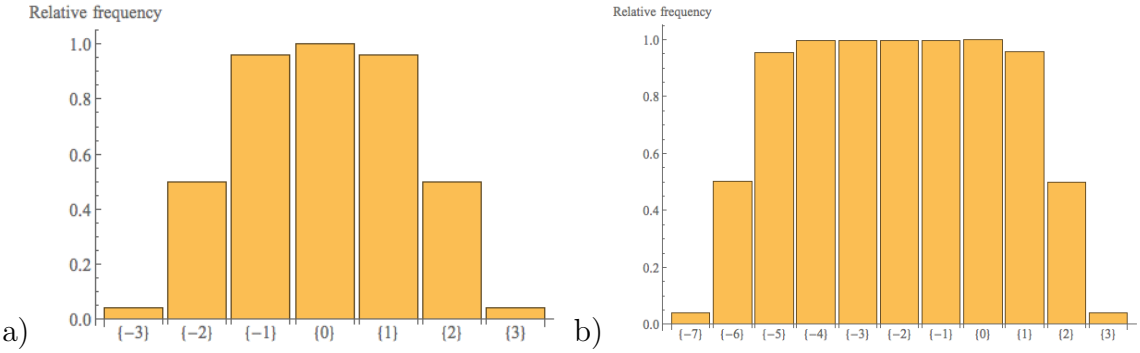

Figure 6. Relative frequencies of single symbols for a) $s = 4$ b) $s = 8$ obtained from time evolution of random initial conditions.

The evolution of frequencies $\mu(\mathsf{M}_\mathcal{R})$ boils down to finding volumes of the polytopes $\mathcal{P}(\mathsf{M}_\mathcal{R})$ determined by the inequalities (62) and (63). Once the volumes are found for all combination of symbols the constant factor $d(\mathcal{R})$ can be extracted from the normalisation condition, by summing up all volumes:

$$d(\mathcal{R})^{-1} = \sum |\mathcal{P}(\mathsf{M}_\mathcal{R})|. \tag{69}$$

For the spatiotemporal cat map the dimension of $\mathcal{P}(\mathsf{M}_\mathcal{R})$ is defined by the length $\partial\mathcal{R}$ of the boundary region (note that for a single cat map $\partial\mathcal{R}$ is always 2). As a result, contrary to the single cat map, the complexity of $|\mathcal{P}(\mathsf{M}_\mathcal{R})|$ calculation grows in general with $|\mathcal{R}|$. Below we illustrate such calculations with 1×1 and 2×2 squares of symbols.

5.4.1. Example: Single symbol frequency. We need to evaluate the volume of the 4-dimensional polytope $\mathcal{P}_m$ for each $m \in \mathcal{A}$. $\mathcal{P}_m$ is defined as the hypercube

$$0 \le x_i < 1, \qquad i = 1, 2, 3, 4 \tag{70}$$

restricted by the condition:

$$m \le x_1 + x_2 + x_3 + x_4 < s + m. \tag{71}$$

The resulting volume depends on m. As can be expected, for $m \in \mathcal{A}_0$ the hyperplane (71) does not intersect cube and the volume $|\mathcal{P}_m|$ is just 1. For "boundary" values $m \in \mathcal{A}_1$ the corresponding volumes $|\mathcal{P}_m|$ are: 1/4!, 1/2 and 23/4!, respectively. The equation (69) yields then $d = s^{-1}$. This gives for frequencies of the symbols from $\mathcal{A}_1$:

$$\mu(\underline{3}) = \mu(s-3) = \frac{1}{24s}, \quad \mu(\underline{1}) = \mu(s-1) = \frac{23}{24s}, \quad \mu(\underline{2}) = \mu(s-2) = \frac{1}{2s}$$

and $\mu(m) = \frac{1}{s}$ for all $m \in \mathcal{A}_0$.

5.4.2. Example: 2×2 block. For the block of four symbols

$$\mathsf{M} = \begin{pmatrix} m_1 & m_2 \\ m_3 & m_4 \end{pmatrix},$$

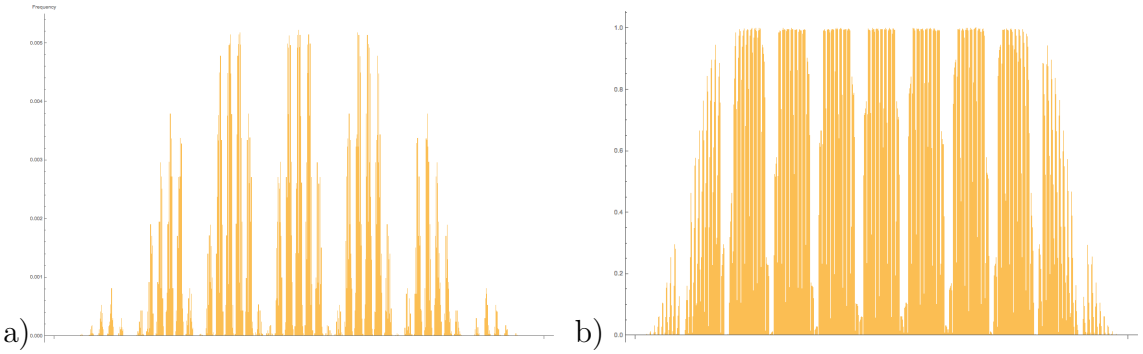

Figure 7. Frequencies of 2×2 spatiotemporal region of symbols for a) $s = 4$ b) $s = 8$ obtained from time evolution of random initial conditions with (57). **To Rana: 1) The axis labels are too small. Make them the same as in fig. 2. 2) As in the single cat case, add explanation on the x-axis.**

the eight dimensional polytope $\mathcal{P}_{\mathsf{M}}$ is defined by $0 \leq x_i < 1, i = 1, \ldots 8$, supplemented by the following inequalities:

$$0 \leq (x_1 + x_8 - m_1)(s^2 - 2) + (x_3 + x_2 + x_6 + x_7 - m_2 - m_3)s + (x_4 + x_5 - m_4)2 \leq \nu_s$$
$$0 \leq (x_2 + x_3 - m_2)(s^2 - 2) + (x_1 + x_8 + x_4 + x_5 - m_1 - m_4)s + (x_7 + x_6 - m_3)2 \leq \nu_s$$
$$0 \leq (x_7 + x_6 - m_3)(s^2 - 2) + (x_1 + x_8 + x_4 + x_5 - m_1 - m_4)s + (x_2 + x_3 - m_2)2 \leq \nu_s$$
$$0 \leq (x_4 + x_5 - m_4)(s^2 - 2) + (x_3 + x_2 + x_6 + x_7 - m_2 - m_3)s + (x_1 + x_8 - m_1)2 \leq \nu_s$$

with $\nu_s = s(s^2 - 4)$. The volumes of $\mathcal{P}_{\mathsf{M}}$ can be evaluated numerically and are found to be consistent with the results obtained by direct simulations of trajectories with random initial conditions and measuring the frequency of a given block M. The corresponding frequencies $\mu(\mathsf{M})$ are presented in figure 7. For $s = 4$ there is only one combination of the internal symbols $m_1 = m_2 = m_3 = m_4 = 0$ which attains the maximum frequency. For $s = 8$ $\mathcal{A}_0$ is composed of 5 symbols and there are 5^4 such combinations. This is reflected in the shape of the histogram in figure 7 (b).

6. Families of invariant 2-tori

By the results of the previous section, it becomes an easy task to obtain a particular class of periodic solutions (i.e., tori) for the spatiotemporal cat map. Since the internal symbols form a full shift, any $N \times T$ block of internal symbols $\mathsf{M} = \{m_z \in \mathcal{A}_0 | z \in \mathbb{Z}^2_{\mathrm{NT}}\}$,

$$\mathbb{Z}^2_{\mathrm{NT}} = \{z = (n, t) | n = 1, \ldots, N, t = 1, \ldots T\},$$

is admissible and generates a periodic solution of (57). Its coordinate representation $\Gamma = \{x_z, z \in \mathbb{Z}^2_{\mathrm{NT}}\}$, is obtained by taking inverse of (57):

$$x_z = \sum_{z' \in \mathbb{Z}^2_{\mathrm{NT}}} \mathsf{g}^0_{z,z'} m_{z'}, \qquad m_{z'} \in \mathcal{A}_0, \tag{72}$$

where $\mathsf{g}^0_{z,z'}$ is the corresponding Green's function with periodic boundary conditions, see Appendix A. This simple procedure can be exploited to test shadowing properties of periodic solutions of the equation (57).

$$\begin{pmatrix}
3&0&0&0&1&1&2&1&1&0&2&3&3&2&2&1&3&1\\
0&1&0&0&3&1&2&1&2&2&3&2&3&3&3&0&2&0\\
2&0&3&1&1&1&3&0&0&2&3&0&3&1&2&2&0&3\\
3&2&0&2&1&3&3&0&0&3&0&3&3&1&3&1&0&2\\
1&2&0&1&\mathbf{0}&\mathbf{1}&\mathbf{2}&\mathbf{0}&\mathbf{3}&\mathbf{1}&\mathbf{2}&\mathbf{2}&2&1&0&1&0&0\\
3&0&0&2&\mathbf{1}&\mathbf{3}&\mathbf{0}&\mathbf{3}&\mathbf{1}&\mathbf{1}&\mathbf{3}&\mathbf{1}&1&1&3&3&0&1\\
2&1&3&3&\mathbf{3}&\mathbf{1}&\mathbf{2}&\mathbf{3}&\mathbf{3}&\mathbf{1}&\mathbf{2}&\mathbf{3}&3&1&2&0&2&0\\
1&1&3&3&\mathbf{3}&\mathbf{2}&\mathbf{0}&\mathbf{3}&\mathbf{0}&\mathbf{2}&\mathbf{2}&\mathbf{3}&0&0&2&3&2&3\\
3&2&1&2&\mathbf{0}&\mathbf{3}&\mathbf{2}&\mathbf{0}&\mathbf{1}&\mathbf{1}&\mathbf{1}&\mathbf{1}&1&2&2&3&2&0\\
0&0&3&1&\mathbf{2}&\mathbf{3}&\mathbf{0}&\mathbf{0}&\mathbf{3}&\mathbf{2}&\mathbf{2}&\mathbf{3}&0&3&1&3&2&0\\
0&1&2&1&\mathbf{2}&\mathbf{0}&\mathbf{1}&\mathbf{2}&\mathbf{3}&\mathbf{0}&\mathbf{3}&\mathbf{3}&0&1&1&3&1&0\\
1&3&3&1&\mathbf{0}&\mathbf{3}&\mathbf{1}&\mathbf{3}&\mathbf{1}&\mathbf{0}&\mathbf{3}&\mathbf{3}&2&1&0&1&0&2\\
0&3&1&3&0&1&2&3&1&1&1&0&1&0&3&1&0&0\\
1&0&3&3&3&1&1&1&1&2&0&2&3&0&0&1&2&1\\
3&2&2&3&2&1&0&0&1&1&2&1&3&0&3&1&2&0\\
1&2&2&0&1&0&3&3&0&3&3&3&0&1&3&1&0&1\\
2&0&2&3&3&3&2&2&0&2&1&3&1&2&0&3&0&1
\end{pmatrix}
\qquad
\begin{pmatrix}
1&0&1&3&1&2&2&1&0&2&3&2&2&0&2&3&2&0\\
3&2&3&3&0&3&2&3&3&2&3&1&2&2&0&1&2&2\\
0&3&3&1&1&1&3&0&0&2&3&0&3&1&0&1&3&1\\
1&3&0&2&1&3&3&0&0&3&0&3&3&1&2&3&3&3\\
1&3&0&1&\mathbf{0}&\mathbf{1}&\mathbf{2}&\mathbf{0}&\mathbf{3}&\mathbf{1}&\mathbf{2}&\mathbf{2}&2&1&3&0&2&2\\
1&1&0&2&\mathbf{1}&\mathbf{3}&\mathbf{0}&\mathbf{3}&\mathbf{1}&\mathbf{1}&\mathbf{3}&\mathbf{1}&1&1&2&0&2&2\\
1&0&3&3&\mathbf{3}&\mathbf{1}&\mathbf{2}&\mathbf{3}&\mathbf{3}&\mathbf{1}&\mathbf{2}&\mathbf{3}&3&1&2&1&1&0\\
1&3&3&3&\mathbf{3}&\mathbf{2}&\mathbf{0}&\mathbf{3}&\mathbf{0}&\mathbf{2}&\mathbf{2}&\mathbf{3}&0&0&2&3&0&0\\
3&1&1&2&\mathbf{0}&\mathbf{3}&\mathbf{2}&\mathbf{0}&\mathbf{1}&\mathbf{1}&\mathbf{1}&\mathbf{1}&1&2&0&2&3&3\\
2&0&3&1&\mathbf{2}&\mathbf{3}&\mathbf{0}&\mathbf{0}&\mathbf{3}&\mathbf{2}&\mathbf{2}&\mathbf{3}&0&3&0&1&3&0\\
0&0&2&1&\mathbf{2}&\mathbf{0}&\mathbf{1}&\mathbf{2}&\mathbf{3}&\mathbf{0}&\mathbf{3}&\mathbf{3}&0&1&2&3&3&0\\
3&1&3&1&\mathbf{0}&\mathbf{3}&\mathbf{1}&\mathbf{3}&\mathbf{1}&\mathbf{0}&\mathbf{3}&\mathbf{3}&2&1&2&3&3&1\\
2&0&1&3&0&1&2&3&1&1&1&0&1&0&1&2&0&2\\
0&0&3&3&3&1&1&1&1&2&0&2&3&0&0&0&2&0\\
1&1&1&2&3&2&3&0&3&0&2&2&2&2&2&3&3&2\\
2&2&3&2&2&1&1&1&0&1&1&1&0&0&0&1&0&3\\
2&1&3&3&2&0&3&0&1&2&0&2&1&2&1&2&1&3
\end{pmatrix}$$

Figure 8. (Color online) 2d symbolic representation of two periodic solutions of (57) shadowing each other within a rectangular region $\mathcal{R}$ (colored in blue) for $s = 7$. The symbols from $\mathcal{R}$ are the same for both solutions and drawn randomly from the internal part of the alphabet $\mathcal{A}_0$. The symbols outside $\mathcal{R}$ are picked up independently and randomly from $\mathcal{A}_0$. The region $\mathcal{R} = \mathcal{R}_0 \cup \mathcal{R}_1$ is separated into internal $\mathcal{R}_0$ (shown in bold font) and the border $\mathcal{R}_1$ parts.

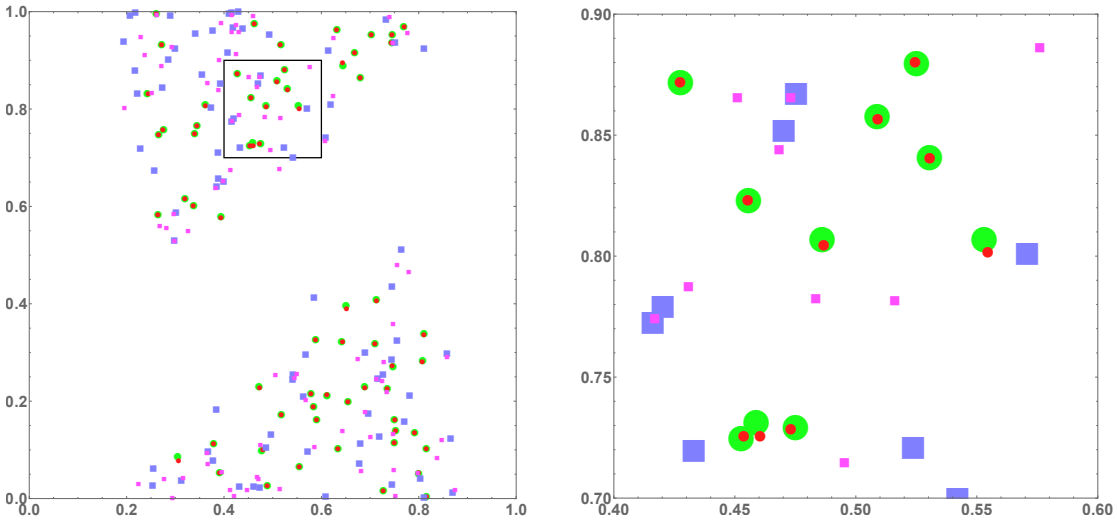

Figure 9. (Color online) On the left - cordinate-momentum representation $(q_z^{(i)}, p_z^{(i)}), i = 1, 2$ of the two periodic solutions (tori) from figure 8. On the right - zoom into small rectangular area shown on the left. Note that the phase space is covered partially, because of using exclusively internal symbols. Only data for $z = (n, t) \in \mathcal{R}$ are shown in the figure. The centers of red (small) circles and green (large) circles are the points $(q_z^{(i)}, p_z^{(i)})$ of the first $(i = 1)$ and the second $(i = 2)$ tori for z's from the interior region $\mathcal{R}_0$. The centers of violet (large) and magenta (small) squares show the respective points from the border $\mathcal{R}_1$ region, see figure 8. It can be clearly observed that all $(q_z^{(1)}, p_z^{(1)})$ and $(q_z^{(2)}, p_z^{(2)})$ from the inner region are well paired, while the distances grow large for z's from $\mathcal{R}_1$. This illustrates the fact that shadowing becomes stronger with the approach to the center of $\mathcal{R}$, see (6).

As the first application, we show in figure 8 two periodic blocks M_Γ, $M_{\Gamma'}$ composed of internal symbols only which coincide at some $\ell \times \ell$ square region $\mathcal{R}$ marked in blue (color on line). In the accompanying figure 9 we show their coordinate representations $\Gamma = \{x_z, z \in \mathbb{Z}^2_{\rm NT}\}$, $\Gamma' = \{x'_z, z \in \mathbb{Z}^2_{\rm NT}\}$ for the spatiotemporal points $z \in \mathcal{R}$. It can be clearly observed that the distances between x_z and x'_z shrink exponentially as z approaches the center of the square. In other words Γ and Γ' shadow each other within the region $\mathcal{R}$.

In the above example Γ and Γ' shadow each other only partially - outside of the region $\mathcal{R}$ their points are not paired. On the other hand, it turns out to be possible to find different periodic solutions of (57) which shadow each other at every point of $\mathbb{Z}^2_{\rm NT}$. Such solutions, referred as partners, play an important role in the semiclassical treatment of the corresponding quantum model, since their action differences are small, see [19–21, 39, 45]. Next, we briefly recall here the construction of partner solutions in 2D setting provided in [21].

Let $\mathsf{M}_\Gamma = \{m_z \in \mathcal{A}_0 | z \in \mathbb{Z}^2_{\rm NT}\}$ be a $N \times T$ symbolic representation of some periodic solution Γ of (57), such that it contains exactly the same block of symbols in several different regions $E = E_1, \dots E_l$ of $\mathbb{Z}^2_{\rm NT}$ which are related by space-time shifts $t \to t + t_i$, $n \to n + n_i$, $i = 1, \dots l$. In other words $\mathsf{M}_\Gamma|_{E_1} = \mathsf{M}_\Gamma|_{E_2} = \dots = \mathsf{M}_\Gamma|_{E_l}$, where $\mathsf{M}_\Gamma|_{E_i}$ stands for the restriction of M_Γ to E_i'th region. Furthermore we will assume that each E_i is a multiply connected region of width ℓ with a non empty interior A_i.§

Such regions $E_i, i = 1, \dots, l$ (called l-encounter) are shown in figure 12 as blue colored regions (color on line). Provided that the interior parts A_i, $i = 1, \dots l$ have different symbolic content i.e., $\mathsf{M}_\Gamma|A_i \neq \mathsf{M}_\Gamma|_{A_j}$ for $i \neq j$, we can construct new periodic solutions of (57) by just permuting symbol regions $\mathsf{M}_\Gamma|_{A_i}, i = 1, \dots, l$. So all together we have $l!$ family of solutions $\Gamma_1, \dots \Gamma_{l!}$ such that their symbolic representations $\mathsf{M}_{\Gamma_1}, \dots \mathsf{M}_{\Gamma_{l!}}$ share the following property - each $\ell \times \ell$ block of the symbols appears one and the same number of times in all of M_{Γ_i}'s. By the shadowing property, this in turn implies that all $\Gamma_1, \dots \Gamma_{l!}$ pass through approximately the same points of the phase space but in different spatiotemporal order. The degree of their closeness is controlled by the parameter ℓ. The larger ℓ is, the closer two different Γ_i, Γ_j come to each other in the phase space. In figure 11 and figure 13 we illustrate these parings for the family of periodic solutions whose symbolic representations are shown in figure 10 and figure 12, respectively.

7. Summary and discussion

In the present paper we have analyzed the linear symbolic dynamics arising in the spatiotemporal cat map (4), coupled along $\mathbb{Z}$ lattice in the regime of full chaos. Bellow we summarize our main results.

§ The width of E_i is defined in the following way. Let A_i and $C_i := \mathbb{Z}^2_{\rm NT} \setminus A_i \cup E_i$ be the interior and exterior of E_i, respectively. We look for all ℓ such that any square $\mathcal{R}$ of the dimension $\ell \times \ell$ having non-zero intersection with A_i i.e., $A_i \cap \mathcal{R} \neq \emptyset$ has zero intersection with C_i i.e., $C_i \cap \mathcal{R} = \emptyset$. The maximum ℓ satisfying this requirement is called width of E_i.

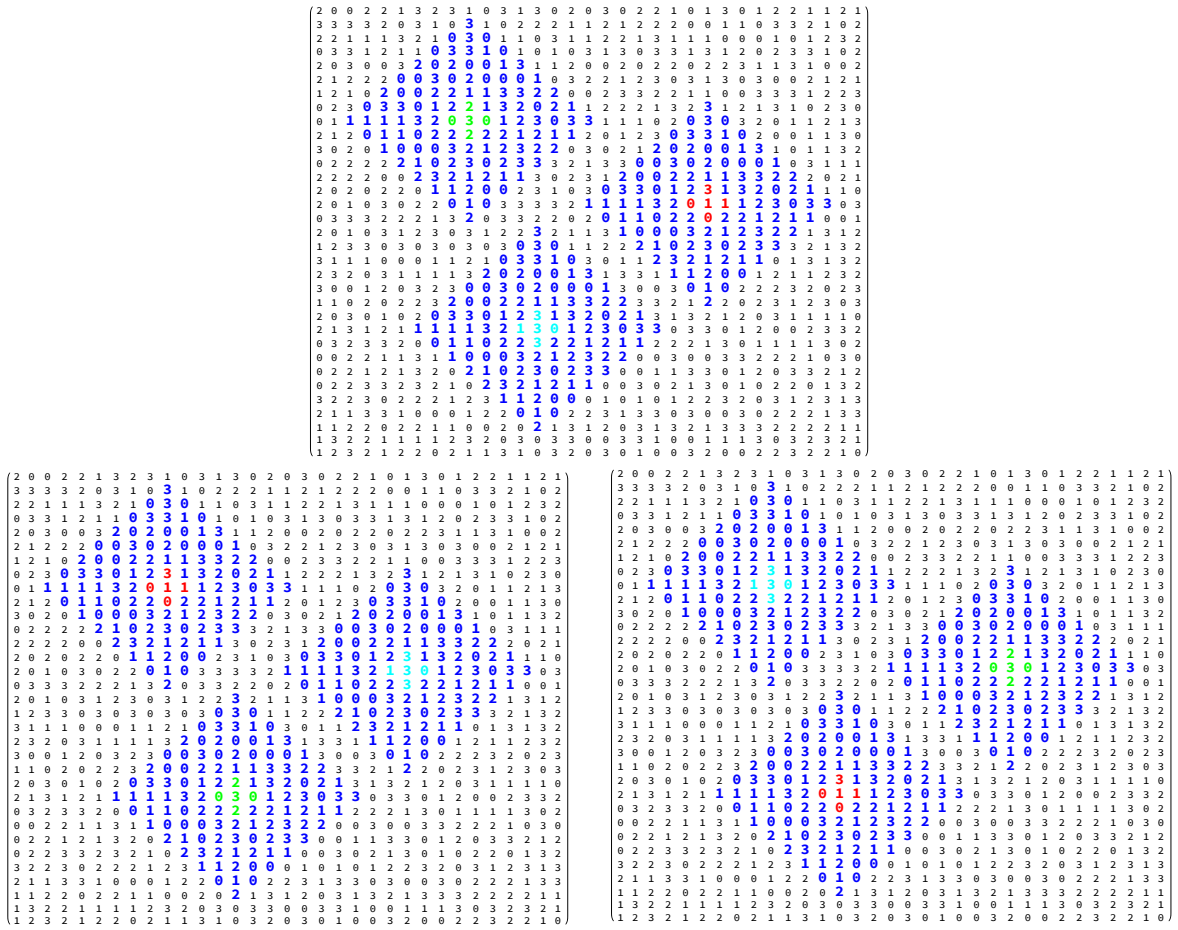

Figure 10. (Color online) Symbolic itineraries of 3 periodic solutions of (57) for $N = 33$, $T = 33$, $s = 7$ which shadow each other at every point. The encounter diamond shaped region of repeated symbols is shown in blue. Three solutions are related by cyclic permutation of inner regions of symbols colored in red, green and light blue, respectively. Any 4×4 block of symbols appears one and the same number of times in both representations.

8. Summary.

The finite alphabet of symbols $\mathcal{A}$ encoding system's dynamics has been shown to split into internal $\mathcal{A}_0$ and exterior $\mathcal{A}_1$ parts, where only symbolic sequences containing external symbols are subject to non-trivial grammar rules. All symbolic blocks composed of internal symbols only, are admissible and attain one and the same frequency for a given block shape $\mathcal{R}$. Furthermore, the frequency of a general block factorizes into product of a constant factor $d_{\mathcal{R}}$ and the geometric one $\mathcal{P}_{\mathcal{R}}$ which can be interpreted as a volume of certain type of polytopes in the Euclidean space whose dimension is determined by the length of the boundary of $\mathcal{R}$. While $d_{\mathcal{R}}$ is fixed by $\mathcal{R}$, $\mathcal{P}_{\mathcal{R}}$ depends on the symbolic content and attains maximum value 1 for blocks of internal symbols. In addition, it has been shown that a local 2D block of symbols determines approximate positions of the corresponding points in the system phase space within an error decreasing exponentially

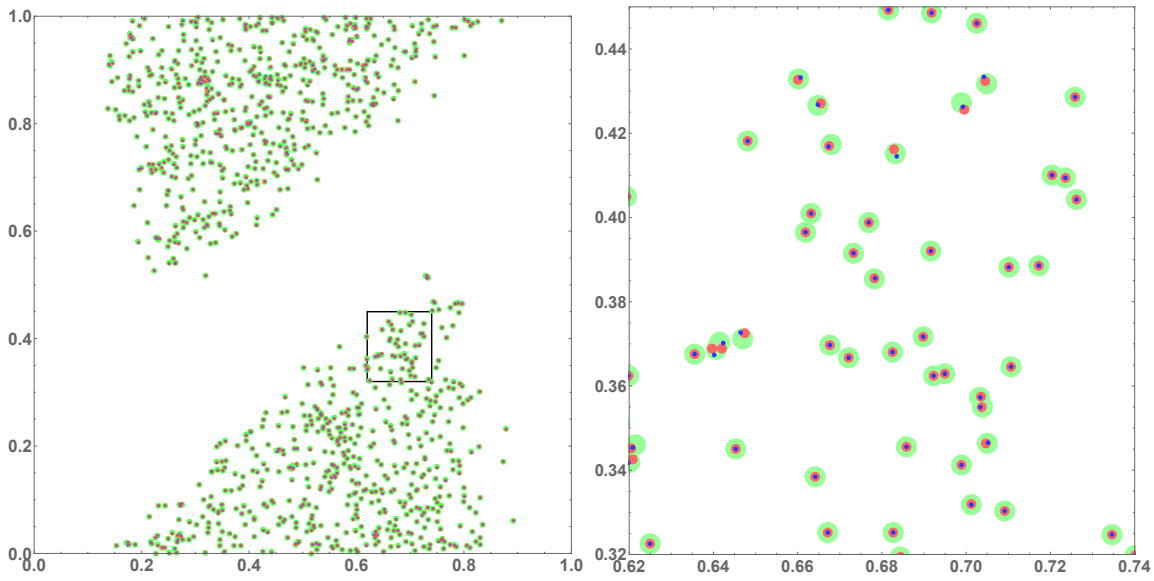

Figure 11. (Color online) Coordinate-momentum representation $(q_z^{(i)}, p_z^{(i)}), i = 1, 2, 3$ of the three periodic solutions (tori) from figure 10 shown as centers of green red and blue circles. Note that the above solutions form almost "perfect" triplets except points from the encounter region, where some deviations can be observed.

$$\begin{pmatrix}
9&1&1&8&4&7&7&0&5&8&1&7&1&0&6&2&1&2&9&6&7\\
4&7&1&0&2&4&4&1&6&5&4&1&3&2&3&3&9&6&9&0&7\\
4&8&3&8&8&6&9&7&1&5&6&6&6&3&3&6&4&6&9&4&0\\
9&0&4&9&5&0&1&9&3&0&8&1&8&0&1&4&7&3&6&3&4\\
2&9&4&9&9&4&1&9&0&1&1&7&4&7&6&3&4&6&8&2&2\\
4&6&3&7&3&5&6&5&1&5&2&6&3&3&0&7&2&2&4&5&6\\
8&1&2&6&6&4&6&2&7&8&3&3&0&0&1&4&3&4&4&1&8\\
2&6&3&1&1&1&0&3&1&7&3&3&6&7&6&6&5&3&2&4&1\\
4&5&6&6&9&5&3&2&5&0&8&4&3&6&1&2&7&9&0&2&9\\
5&7&3&6&1&1&1&0&2&3&9&5&3&7&5&0&5&9&0&8&7\\
5&7&6&3&9&5&5&3&3&4&8&1&6&5&3&9&6&5&4&1&3\\
1&6&3&7&6&5&9&3&2&3&1&2&9&0&3&8&7&3&3&0&6\\
1&3&4&3&0&2&8&0&6&2&1&7&9&1&5&7&5&1&2&2&0\\
0&6&3&7&8&2&1&1&1&0&8&3&8&8&6&9&7&1&4&0&4\\
0&5&3&4&9&7&4&7&7&9&0&4&9&5&0&1&9&3&2&3&6\\
3&5&2&9&8&3&9&0&7&9&9&4&9&9&4&1&9&0&0&6&8\\
1&5&2&7&4&1&6&8&5&4&6&3&7&2&7&6&5&1&8&8&7\\
9&4&1&6&6&7&1&1&8&9&1&2&6&1&7&6&2&7&2&2&5\\
5&7&1&0&3&3&3&0&6&9&6&3&1&9&2&0&3&1&9&3&2\\
6&1&2&1&1&0&5&0&6&6&5&6&6&9&5&3&2&5&6&4&4\\
1&9&9&2&0&8&6&7&5&9&7&3&6&1&1&1&0&2&8&2&1\\
3&1&8&3&4&3&6&1&9&8&7&6&3&9&5&5&3&3&6&2&3\\
6&2&1&7&6&7&7&3&5&9&4&7&5&5&1&2&9&0&8&6&9\\
7&8&8&9&6&1&1&4&9&3&8&5&4&8&4&2&1&6&3&7&9\\
5&8&7&5&3&8&7&1&8&0&8&5&4&3&0&4&0&3&4&1&7
\end{pmatrix}
\quad
\begin{pmatrix}
9&1&1&8&4&7&7&0&5&8&1&7&1&0&6&2&1&2&9&6&7\\
4&7&1&0&2&4&4&1&6&5&4&1&3&2&3&3&9&6&9&0&7\\
4&8&3&8&8&6&9&7&1&5&6&6&6&3&3&6&4&6&9&4&0\\
9&0&4&9&5&0&1&9&3&0&8&1&8&0&1&4&7&3&6&3&4\\
2&9&4&9&9&4&1&9&0&1&1&7&4&7&6&3&4&6&8&2&2\\
4&6&3&7&2&7&6&5&1&5&2&6&3&3&0&7&2&2&4&5&6\\
8&1&2&6&1&7&6&2&7&8&3&3&0&0&1&4&3&4&4&1&8\\
2&6&3&1&9&2&0&3&1&7&3&3&6&7&6&6&5&3&2&4&1\\
4&5&6&6&9&5&3&2&5&0&8&4&3&6&1&2&7&9&0&2&9\\
5&7&3&6&1&1&1&0&2&3&9&5&3&7&5&0&5&9&0&8&7\\
5&7&6&3&9&5&5&3&3&4&8&1&6&5&3&9&6&5&4&1&3\\
1&6&3&7&6&5&9&3&2&3&1&2&9&0&3&8&7&3&3&0&6\\
1&3&4&3&0&2&8&0&6&2&1&7&9&1&5&7&5&1&2&2&0\\
0&6&3&7&8&2&1&1&1&0&8&3&8&8&6&9&7&1&4&0&4\\
0&5&3&4&9&7&4&7&7&9&0&4&9&5&0&1&9&3&2&3&6\\
3&5&2&9&8&3&9&0&7&9&9&4&9&9&4&1&9&0&0&6&8\\
1&5&2&7&4&1&6&8&5&4&6&3&7&3&5&6&5&1&8&8&7\\
9&4&1&6&6&7&1&1&8&9&1&2&6&6&4&6&2&7&2&2&5\\
5&7&1&0&3&3&3&0&6&9&6&3&1&1&1&0&3&1&9&3&2\\
6&1&2&1&1&0&5&0&6&6&5&6&6&9&5&3&2&5&6&4&4\\
1&9&9&2&0&8&6&7&5&9&7&3&6&1&1&1&0&2&8&2&1\\
3&1&8&3&4&3&6&1&9&8&7&6&3&9&5&5&3&3&6&2&3\\
6&2&1&7&6&7&7&3&5&9&4&7&5&5&1&2&9&0&8&6&9\\
7&8&8&9&6&1&1&4&9&3&8&5&4&8&4&2&1&6&3&7&9\\
5&8&7&5&3&8&7&1&8&0&8&5&4&3&0&4&0&3&4&1&7
\end{pmatrix}$$

Figure 12. (Color online) Symbolic itineraries of 2 periodic solutions of (57) for $N = 25$, $T = 25$, $s = 13$ which shadow each other at every point. The encounter region of repeated symbolic block-like region is shown in blue. The two solutions are related by permutation of inner regions of symbols colored in red and blue, respectively. Any 4×4 block of symbols appears one and the same number of times in both representations.

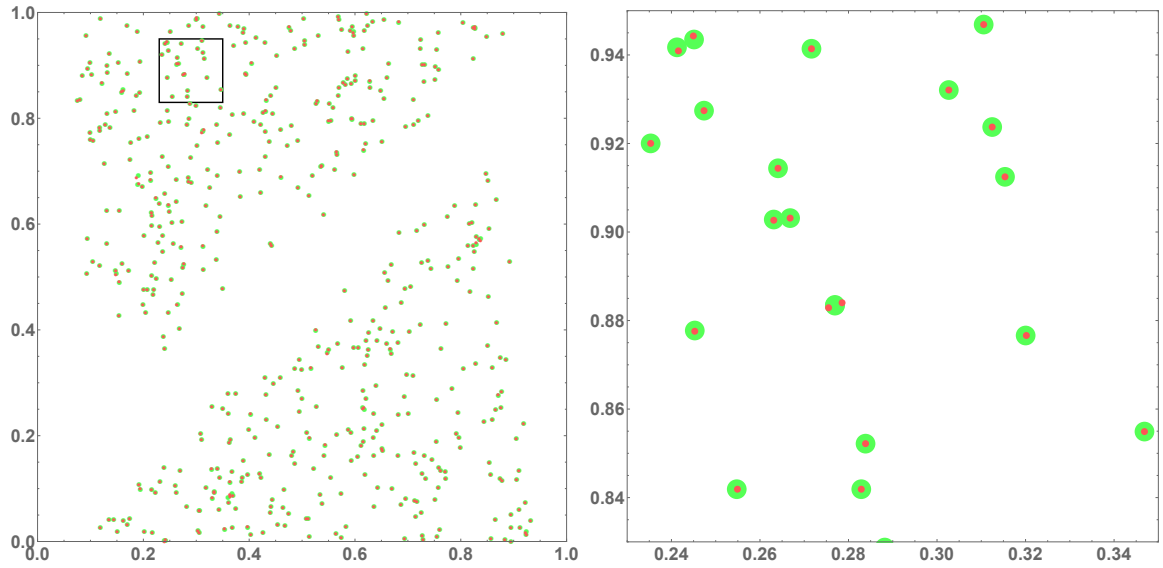

Figure 13. (Color online) Coordinate-momentum representation $(q_z^{(i)}, p_z^{(i)}), i = 1, 2$ of the two periodic solutions (tori) from figure 12.

with the size of the block.

As an application of these results we have constructed an example of partner periodic tori composed of internal symbols which pass through approximately the same positions in the phase space, but in different spatio-temporal "order". Such periodic tori shadowing each other everywhere are expected to play an important role in the semiclassical treatment of the corresponding quantum models.

8.1. Discussion.

The alphabet separation into internal and external parts nicely illustrates the transition of the model from the correlated regime to the uncorrelated Bernoulli process as parameter s in (4) tends to ∞. Indeed, the number of external symbols in $\mathcal{A}_1$ is fixed within a given differential operator $\Box$ structure, while the number of internal symbols in $\mathcal{A}_0$ grows linearly with the parameter s controlling the strength of chaos in a single map. For single cat map this transition can be achieved by merely increasing the time step of time evolution. Increasing the time step from 1 to 2 leaves the form of equation (22) intact, but renormalizes the constant $s \to s^2 - 1$. This reflects the fact that ϕ^2 is more "chaotic" than ϕ. With an increase of k the map ϕ^k resembles more and more uncorrelated Bernoulli process. Similar transition can be observed in the coupled $\mathbb{Z}$ map lattices, with a caveat that switch from Φ to Φ^k renormalizes not only the constant s, but $\Box$ itself. The resulting equation of motion will contain an elliptic operator $\Box^{(k)}$ of higher order. Still, it is straightforward to see that the number of external symbols is controlled by the order of the operator $\Box^{(k)}$ which grows linearly with k. On the other hand, the number of internal symbols grows in the same way as the constant s i.e., exponentially.

Remarkably, as far as the linear symbolic dynamics is concerned, the above results hold both for single cat map and their coupled lattice $\mathbb{Z}$ extension. As a matter of fact, their proofs essentially rely only upon ellipticity of the operator $\Box$ and the linear structure of equation. Therefore, it is very plausible that the same results hold for the lattices $\mathbb{Z}^d$ of an arbitrary dimension d. Furthermore, the restriction to the integer valued matrices which define the map seems to be unnecessary. Cat map is a particular (smooth) version of the saw map which is defined by the same equation (22), but a general (not necessarily integer) value of s. The linear symbolic dynamics for single saw map has been analyzed in [40] and its extension to a coupled $\mathbb{Z}^d$ model along the lines of the present paper seems to be straightforward. Also, in the current paper we sticked to the Laplacian form of $\Box$. Again this seems to be too restrictive and extension to other elliptic operators of higher order should be possible. Such operators are necessarily appear within the models with higher range of interactions.

A non-trivial way to extend current setting would be inclusion of an external potential $\mathcal{V}$ breaking down the linear structure of (4)

$$(\Box - s + 2d + \mathcal{V}'(z))x_z = m_z, \qquad z \in \mathbb{Z}^d. \tag{73}$$

As far as perturbation $\mathcal{V}$ is weak enough, the resulting lattice map should be conjugated to a linear one where $\mathcal{V} = 0$. This approach has been already exploited in [21] to construct partner invariant 2-tori for perturbed cat map lattices. On the other hand, for a larger perturbation strength such a conjugation to linear system should not be possible anymore. Finally, let us note that the lattice models like (73) can be seen as discretized versions of PDEs arising from the Hamiltonian field theories. In this respect it would be of interest to study, whether any of the present results can be extended to the continues, PDE setting. In particular, the following questions seem to be of fundamental importance:

- Can an effective 2D symbolic dynamics with finite alphabet be constructed for any example of PDE with spatio-temporal chaos, such that a) Connection between periodic field solutions and their symbolic representation is unique; b) The local symbolic content would define the values of the corresponding fields with the exponentially decreasing errors?
- Is the phenomenon of shadowing between periodic field solutions is generic for PDE with spatio-temporal chaos? In other words, can solutions of such PDE be separated into families, where all elements shadow each other at every space time point? What is the role of such pairings in the corresponding quantum field theories?

In past decade hundreds of such solutions been computed for a variety of flow geometries, always confined to small computational regions (minimal cells). While the setting is classical, such classical field-theory advances offer new semi-classical approaches to quantum field theory and many-body problems.

There is much to say about the cat map quantization, starting with the work of Hannay and Berry [22], the analysis of the use of the periodic orbits of the cat map

in its quantization by Keating [13, 29], and subsequent developments such as Keating and Mezzadri [30, 31], but in present work we shall restrict our considerations to purely classical deterministic spatiotemporal dynamics.

Acknowledgments

We are grateful to XXX, and XXX for many fruitful discussions. Work of B. G. and P. C. was supported by the family of late G. Robinson, Jr..

Appendix A. Green's functions for $\mathbb{Z}^1$ and $\mathbb{Z}^2$ lattices

Appendix A.1. $\mathbb{Z}^1$ Green's function.

$$(-\Box + s - 2)g_t = \delta_{t,0}, \qquad t \in \mathbb{Z}^1\,. \tag{A.1}$$

For single cat map the corresponding Green's function is given by:

$$g_n = \frac{1}{\pi}\int_0^\pi \frac{\cos(nx)}{s - 2\cos x}dx = \Lambda^{-|n|}/(\Lambda - \Lambda^{-1}),$$

with $s = \Lambda + \Lambda^{-1}$, $\Lambda > 1$.

Periodic boundary conditions. The Green's function for periodic boundary conditions is easy to find by using g_n:

$$\tilde{g}_n = \sum_{j=-\infty}^{\infty} g_{n-jT} = \frac{\Lambda^{-|n|} + \Lambda^{-|n-T|}}{(1-\Lambda^{-T})(\Lambda - \Lambda^{-1})}.$$

Dirichlet boundary conditions. It is possible to find g in two different ways. 1st one is to use inverse matrices. Here $\mathcal{D}$ is tridiagonal matrix of the size $\ell \times \ell$:

$$\mathcal{D} = \begin{pmatrix} s & -1 & 0 & 0 & \dots & 0 & 0 \\ -1 & s & -1 & 0 & \dots & 0 & 0 \\ 0 & -1 & s & -1 & \dots & 0 & 0 \\ \vdots & \vdots & \vdots & \vdots & \ddots & \vdots & \vdots \\ 0 & 0 & \dots & \dots & \dots & -1 & s \end{pmatrix}.$$

The matrix elements of $\mathcal{D}^{-1}$ can be expressed through the Chebyshev polynomials $u_n(s/2) = \frac{\sinh(n+1)\lambda}{\sinh\lambda}$, $s = 2\cosh\lambda$:

$$\mathsf{g}_{i,j} = (\mathcal{D}^{-1})_{i,j} = \begin{cases} \frac{u_{i-1}(s/2)u_{\ell-j}(s/2)}{u_\ell(s/2)}, & \text{for } i \le j \\ \frac{u_{j-1}(s/2)u_{\ell-i}(s/2)}{u_\ell(s/2)}, & \text{for } i > j. \end{cases} \tag{A.2}$$

The 2nd way to evaluate $\mathsf{g}_{i,j}$ is to use Green's function g and take antiperiodic sum (analogous to periodic boundary conditions). This approach can be easily extended to $\mathbb{Z}^2$ case.

Note that for all boundary conditions the Green's function turns out to be strictly negative.

Appendix A.2. $\mathbb{Z}^2$ Green's function.

The Green's function $g(z,z') = g(z-z',0) =: g_{n,t}$, $z-z' = (n,t) \in \mathbb{Z}^2$ solves the equation:

$$(-\Box + s - 4)g_{n,t} = \delta_{n,0}\delta_{t,0}. \tag{A.3}$$

The solution is given by the double integral:

$$g_{n,t} = \frac{1}{\pi^2}\int_0^\pi \int_0^\pi \frac{\cos(nx)\cos(ty)}{s - 2\cos x - 2\cos y} dxdy. \tag{A.4}$$

In particular, the diagonal elements can be calculated explicitly [36]:

$$g_{n,n} = \frac{-1}{4\pi i}\left(2iQ_{n-1/2}(z) + \pi P_{n-1/2}(z)\right), \quad z = s^2/8 - 1 > 1.$$

References

[1] R. L. Adler and B. Weiss, "Entropy, a complete metric invariant for automorphisms of the torus", Proc. Natl. Acad. Sci. USA **57**, 1573–1576 (1967).

[2] R. L. Adler and B. Weiss, *Similarity of automorphisms of the torus*, Vol. 98, Memoirs Amer. Math. Soc. (Amer. Math. Soc., Providence RI, 1970).

[3] V. I. Arnol'd and A. Avez, *Ergodic Problems of Classical Mechanics* (Addison-Wesley, Redwood City, 1989).

[4] R. Bowen, *Equilibrium States and the Ergodic Theory of Anosov Diffeomorphisms* (Springer, Berlin, 1975).

[5] F. Brini, S. Siboni, G. Turchetti, and S. Vaienti, "Decay of correlations for the automorphism of the torus T^2", Nonlinearity **10**, 1257–1268 (1997).

[6] L. A. Bunimovich and Y. G. Sinai, "Spacetime chaos in coupled map lattices", Nonlinearity **1**, 491 (1988).

[7] B. V. Chirikov, "A universal instability of many-dimensional oscillator system", Phys. Rep. **52**, 263–379 (1979).

[8] F. Christiansen, P. Cvitanović, and V. Putkaradze, "Spatiotemporal chaos in terms of unstable recurrent patterns", Nonlinearity **10**, 55–70 (1997).

[9] S. C. Creagh, "Quantum zeta function for perturbed cat maps", Chaos **5**, 477–493 (1995).

[10] P. Cvitanović and J. F. Gibson, "Geometry of turbulence in wall-bounded shear flows: Periodic orbits", Phys. Scr. T **142**, 014007 (2010).

[11] P. Cvitanović, R. L. Davidchack, and E. Siminos, "On the state space geometry of the Kuramoto-Sivashinsky flow in a periodic domain", SIAM J. Appl. Dyn. Syst. **9**, 1–33 (2010).

[12] P. Cvitanović, R. Artuso, R. Mainieri, G. Tanner, and G. Vattay, *Chaos: Classical and Quantum* (Niels Bohr Inst., Copenhagen, 2016).

[13] I. Dana, "General quantization of canonical maps on a two-torus", J. Phys. A **35**, 3447 (2002).

[14] R. L. Devaney, *An Introduction to Chaotic Dynamical systems*, 2nd ed. (Westview Press, 2008).

[15] X. Ding, H. Chaté, P. Cvitanović, E. Siminos, and K. A. Takeuchi, "Estimating the dimension of the inertial manifold from unstable periodic orbits", Phys. Rev. Lett. **117**, 024101 (2016), `arXiv:1604.01859`.

[16] I. García-Mata and M. Saraceno, "Spectral properties and classical decays in quantum open systems", Phys. Rev. E **69**, 056211 (2004).

[17] G. Giacomelli, S. Lepri, and A. Politi, "Statistical properties of bidimensional patterns generated from delayed and extended maps", Phys. Rev. E **51**, 3939–3944 (1995).

[18] F. Ginelli, P. Poggi, A. Turchi, H. Chaté, R. Livi, and A. Politi, "Characterizing dynamics with covariant Lyapunov vectors", Phys. Rev. Lett. **99**, 130601 (2007), http://arXiv.org/abs/0706.0510.

[19] B. Gutkin and V. Osipov, "Clustering of periodic orbits and ensembles of truncated unitary matrices", J. Stat. Phys. **153**, 1049–1064 (2013).

[20] B. Gutkin and V. Osipov, "Clustering of periodic orbits in chaotic systems", Nonlinearity **26**, 177 (2013).

[21] B. Gutkin and V. Osipov, "Classical foundations of many-particle quantum chaos", Nonlinearity **29**, 325–356 (2016).

[22] J. H. Hannay and M. V. Berry, "Quantization of linear maps on a torus – Fresnel diffraction by a periodic grating", Physica D **1**, 267–290 (1980).

[23] B. Hof, C. W. H. van Doorne, J. Westerweel, F. T. M. Nieuwstadt, H. Faisst, B. Eckhardt, H. Wedin, R. R. Kerswell, and F. Waleffe, "Experimental observation of nonlinear traveling waves in turbulent pipe flow", Science **305**, 1594–1598 (2004).

[24] W. G. Hoover and K. Aoki, Order and chaos in the one-dimensional ϕ^4 model : N-dependence and the Second Law of Thermodynamics, 2016.

[25] S. Isola, "ζ-functions and distribution of periodic orbits of toral automorphisms", Europhys. Lett. **11**, 517–522 (1990).

[26] K. Kaneko, "Transition from torus to chaos accompanied by frequency lockings with symmetry breaking: In connection with the coupled-logistic map", Prog. Theor. Phys. **69**, 1427–1442 (1983).

[27] K. Kaneko, "Period-doubling of kink-antikink patterns, quasiperiodicity in antiferro-like structures and spatial intermittency in coupled logistic lattice: Towards a prelude of a "field theory of chaos"", Prog. Theor. Phys. **72**, 480–486 (1984).

[28] H. Kantz and P. Grassberger, "Chaos in low-dimensional Hamiltonian maps", Phys. Let. A **123**, 437–443 (1987).

[29] J. P. Keating, "The cat maps: quantum mechanics and classical motion", Nonlinearity **4**, 309–341 (1991).

[30] J. P. Keating and F. Mezzadri, "Pseudo-symmetries of Anosov maps and spectral statistics", Nonlinearity **13**, 747–775 (2000).

[31] J. P. Keating, F. Mezzadri, and J. M. Robbins, "Quantum boundary conditions for torus maps", Nonlinearity **12**, 579 (1999).

[32] T. Kreilos and B. Eckhardt, "Periodic orbits near onset of chaos in plane Couette flow", Chaos **22**, 047505 (2012), http://arXiv.org/abs/1205.0347.

[33] S. Lepri, A. Politi, and A. Torcini, "Chronotopic Lyapunov analysis. I. A detailed characterization of 1D systems", J. Stat. Phys. **82**, 1429–1452 (1996).

[34] S. Lepri, A. Politi, and A. Torcini, "Chronotopic Lyapunov analysis. II. Towards a unified approach", J. Stat. Phys. **88**, 31–45 (1997).

[35] A. J. Lichtenberg and M. A. Lieberman, *Regular and Chaotic Dynamics*, 2nd ed. (Springer, New York, 2013).

[36] P. A. Martin, "Discrete scattering theory: Green's function for a square lattice", Wave Motion **43**, 619–629 (2006).

[37] B. D. Mestel and I. Percival, "Newton method for highly unstable orbits", Physica D **24**, 172 (1987).

[38] J. Milnor and W. Thurston, "Iterated maps of the interval", in *Dynamical Systems (Maryland 1986-87)*, edited by A. Dold and B. Eckmann (Springer, New York, 1988), pp. 465–563.

[39] S. Müller, S. Heusler, P. Braun, F. Haake, and A. Altland, "Semiclassical foundation of universality in quantum chaos", Phys. Rev. Lett. **93**, 014103 (2004).

[40] I. Percival and F. Vivaldi, "A linear code for the sawtooth and cat maps", Physica D **27**, 373–386 (1987).

[41] I. Percival and F. Vivaldi, "Arithmetical properties of strongly chaotic motions", Physica D **25**, 105–130 (1987).

[42] Y. B. Pesin and Y. G. Sinai, "Space-time chaos in the system of weakly interacting hyperbolic systems", J. Geom. Phys. **5**, 483–492 (1988).

[43] A. Politi, A. Torcini, and S. Lepri, "Lyapunov exponents from node-counting arguments", J. Phys. IV **8**, 263 (1998).

[44] D. Ruelle, "A measure associated with Axiom-A attractors", Amer. J. Math. **98**, 619–654 (1976).

[45] M. Sieber and K. Richter, "Correlations between periodic orbits and their rle in spectral statistics", Phys. Scr. **2001**, 128 (2001).

[46] Y. G. Sinai, "On the concept of entropy of a dynamical system", Dokl. Akad. Nauk. SSSR **124**, 768–771 (1959).

[47] J. Slipantschuk, O. F. Bandtlow, and W. Just, Complete spectral data for analytic Anosov maps of the torus, 2016.

[48] R. Sturman, J. M. Ottino, and S. Wiggins, *The Mathematical Foundations of Mixing*, Cambridge Monographs on Applied and Computational Mathematics (Cambridge Univ. Press, 2006).

[49] A. P. Willis, P. Cvitanović, and M. Avila, "Revealing the state space of turbulent pipe flow by symmetry reduction", J. Fluid Mech. **721**, 514–540 (2013).

[50] A. Wirzba and P. Cvitanović, "Appendix: Discrete symmetries of dynamics", in *Chaos: Classical and Quantum* (Niels Bohr Inst., Copenhagen, 2016).

[51] A. Zee, *Quantum Field Theory in a Nutshell*, 2nd ed. (Princeton Univ. Press, Princeton NJ, 2010).